Marine faunas of the Preboreal stage in the Oslo area

Renate Rosseland Johansen

Thesis submitted for the degree of Master of Sciences
in Sedimentology, Paleontology and Stratigraphy
60 credits

Department of Geoscience
Faculty of Mathematics and Natural Sciences
And
Natural History Museum

UNIVERSITY OF OSLO

June 2020

Supervisors: Øyvind Hammer (UiO/NHM), Hans Arne Nakrem (UiO/NHM)

2020

Marine faunas of the Preboreal stage in the Oslo area

http://www.duo.uio.no/

Trykk: Reprosentralen, Universitetet i Oslo

Abstract

The early Holocene marine faunas of the Oslo area were studied in classical works by Brøgger (1901) and others, but there has been relatively little research in recent decades. Classical fossil localities near the marine limit at ca. 220m above sea level around Oslo are now difficult to localize, overgrown or completely lost and it is difficult to collect new material. However, the material of Brøgger, Øyen and others can be studied in the extensive Quaternary collections of the Natural History Museum in Oslo. The historical locality in Skådalen at the marine limit, new datings of *Mytilus edulis* 10,260 ± 70 ^{14}C years and *Balanus* 6200 ± 40 ^{14}C years were done in this thesis. Both samples seemingly from the same locality but the ages do not correspond. Holtedahl (1960) encountered the same problem when dating the same locality. For the Sognsvann locality *Mytilus edulis* were dated 10,150 ± 70 ^{14}C years, corresponding well with the timeline created in this thesis, both Sognsvann and Skådalen samples are seemingly collected outside the main ridges of the Aker substage. Also, Vardeåsen, Nesodden locality, *Mya* were dated 9915 ± 50 ^{14}C years. CT scanning, isotope profiling (δ^{18}O) and LA-ICPMS analysis were performed on *Mytilus edulis* from the Skådalen and Sognsvann locality showing evidence of freshwater input and seasonal changes in Ba values correspond well with seasonal changes in δ^{18}O. SEM imaging of ostracods from the Sognsvann location made it possible to identify species and further enhance the possibility of freshwater input, placing the locality close to the ice front. The Preboreal Oscillation is suggested to be related to either the Ås – Ski substage or the Aker substage, the connection with the Aker substage being more likely.

Acknowledgment

I would like to express my gratitude to my supervisors Øyvind Hammer and Hans Arne Nakrem for sharing their knowledge and helping me throughout my thesis. After the COVID-19 outbreak they were quick to answer the excessive amounts of e-mails I sent. I appreciate all your help and cannot thank you enough.

A big thank you to Magnus Kristoffersen for helping with the LA-ICPMS analyses, both the execution and calculations afterwards. Nélia Castro for helping with the beautiful SEM images of the ostracods. I would also like to thank Jan Kornstad for collecting material from Vardeåsen, Nesodden and letting me use the material in this thesis.

Of course, family who was there with encouraging words and unconditional support throughout these two intense years. Britt H. Volden for helping with proofreading and my fiancé Magnus H. Volden who helped with proofreading and never stopped believing in me.

Table of contents

1 Introduction

1.1 Aim of the study

The aim is to study the age and paleoenvironment of the marine limit in the Oslo area during the earliest Holocene, ~10,000 years ago. This area has not been studied in detail since Brøgger did an extensive study and published his results in 1901, and many of the historical locations are lost. This thesis therefore focuses on works of other authors for comparison with present day knowledge of species habitat. Some new radiocarbon datings are introduced, and elemental and isotopic profiling of shells is attempted as a tool for environmental reconstruction. A previously undescribed ostracod fauna from a locality south of Sognsvann is also described and interpreted.

1.2 Chapter introduction

Chapter 1 – Introduction provides an introduction of the Oslofjord area and a description of each of the stages created by melting of the icecap: The Ra substage, the Ås-Ski substage and the Aker substage. The focus further in this thesis will be the Aker substage.

Chapter 2 – Materials and Methods gives a short introduction of the localities studied in this thesis and a table of abbreviations used. A short summary of the different methods of analysis used for the different samples.

Chapter 3 – Results presents the results from the different analyses.

Chapter 4 – Discussion combines and incorporates the obtained results with existing knowledge of the Aker substage.

Chapter 5 – Conclusion sums up the most important findings and outcomes of the thesis.

1.3 The Oslo area

Norway has been through many ice-ages, as evident by its rocky landscape, U-shaped valleys and sharp mountain-peaks. Ice has shaped the Norwegian landscape for millions of years, but the most recent glaciation (Weichselian) occurred between 115,000 and 11,700 years ago. After this last glaciation an interglacial period followed, this epoch is known as the Holocene. The global temperature during the early Holocene was close to present temperatures, before reaching its maximum in Western Europe around 6000 B.P. (Davis et al., 2003).

The different substages of the glacier retreat in the Oslo area during the earliest Holocene have been studied. The three stages during the deglaciation, the Ra substage, the Ås-Ski substage and the Aker substage, are identified in Brøgger's clay deposits (Table 1.1) and have been compared to Feyling-Hanssen's foraminiferal zones (Table 1.3). This thesis aims to give further information about the environment of deposition during the Aker substage in particular. Locations investigated from the Aker substage are shown in Figs. 1.1 and 1.2. Full names of all species mentioned in this thesis can be found in Appendix 6 and abbreviations used can be found in Table 2.1 in chapter Materials and Method 2.1.

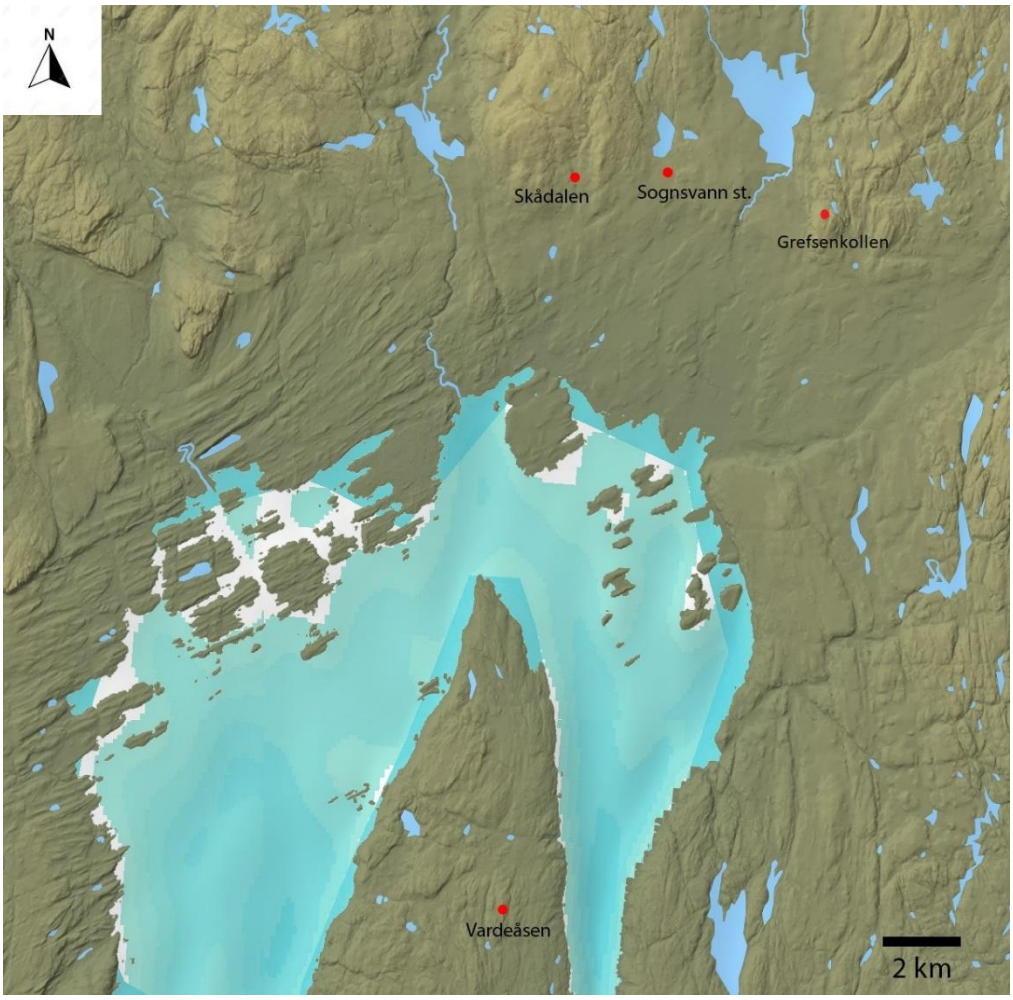

Fig. 1.1. An overview of the Oslofjord area with locations of sampling shown with red dots and the name of the location. Map is modified from norgeskart.no.

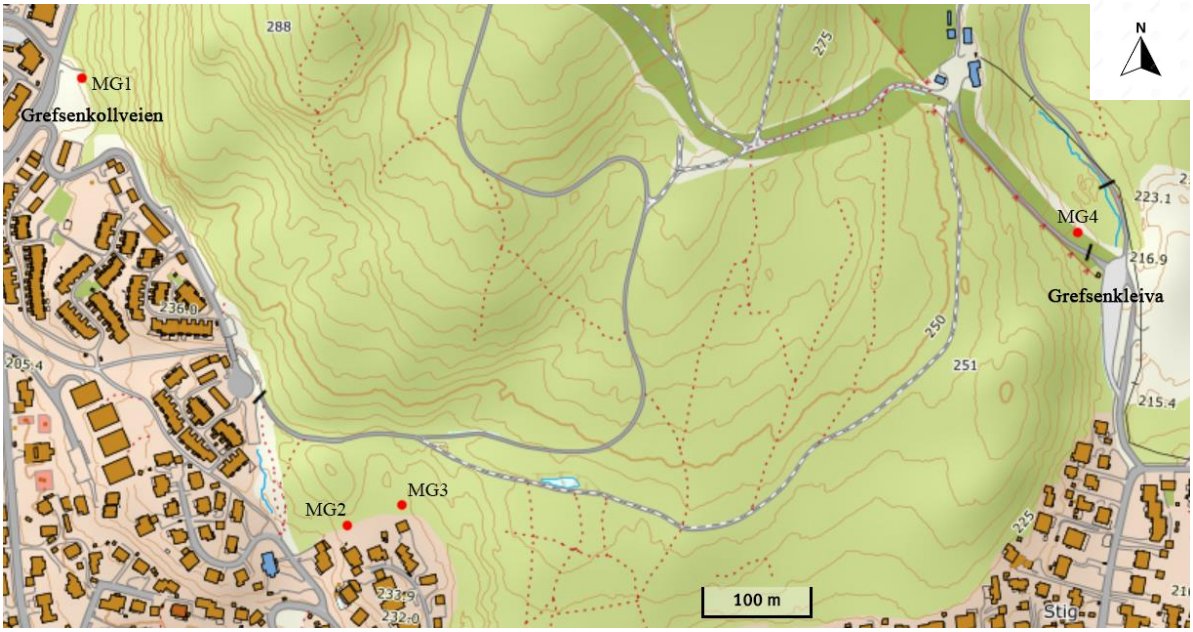

Fig. 1.2. An overview of Grefsenkollen with locations of sampling shown with red dots and the name of the sample. Map is modified from norgeskart.no.

Brøgger (1901) investigated the stratigraphy and paleoclimatic indicators of the late Quaternary deposits in the Oslofjord area. The shallow-water deposits were divided into 6 shell beds and the deeper clay sediments into 12 zones based on their fossil content (Feyling-Hanssen, 1964). The 12 clay zones are all named after a characteristic species dominating the deposit. Table 1.1 shows the zones from oldest to youngest with their characterizing species and where they were deposited (Feyling-Hanssen, 1964).

Further Feyling-Hanssen (1964) investigated numerous borings through late Quaternary deposits of the northern parts of the Oslofjord, especially from the city of Oslo. From his results he identified seven zones of foraminifera deposited under different conditions. Table 1.2 shows the different foraminiferal zones with their dominant species and where they were deposited. Holtedahl (1960) made a comparison between Brøgger's clay zones and Feyling-Hanssen's foraminiferal zonation.

There are three moraine ridges evident in the Oslofjord area. The three moraine ridges identified are the Ra substage, the Ås-Ski substage and the Aker substage. Each substage is defined by a moraine ridge and the fauna present in and around the moraines (Fig. 1.3, Table 1.1; Brøgger, 1901).

Table 1.1. An overview of the clay deposits described by Brøgger (1901), the different species defining each unit (Feyling-Hanssen, 1964, with taxa revised from Brøgger, 1901), where each clay unit was deposited geographically and a list of some radiocarbon datings from Holtedahl (1960).

Clay deposits	**Defining species from Feyling – Hanssen (1964). (Taxon used by Brøgger, 1901)**	**Deposited**	**Datings, uncalibrated (Holtedahl, 1960)**
Yoldia clay	*Portlandia arctica* *(= Yoldia arctica)*	South of the Ra ridge	9950 ± 300 yr and 9921 ± 220 yr
Subdivided into: Older Yoldia clay Younger Yoldia clay			
Arca clay	*Bathyarca glacialis* *(=Arca glacialis)*	As the ice front retreated from the Ra to the Ås-Ski moraines	
Subdivided into: Older Arca clay Middle Arca clay Older Portlandia clay			Middle Arca clay: 9750 ± 250 yr
Younger Arca clay and Portlandia clay	*Yoldiella lenticula* *(=Portlandia lenticula)*	Continued retreat of the ice margin to the moraines of the Aker substage	
Youngest Arca- and Portlandia clay	*Yoldiella lenticula* *(=Portlandia lenticula)*	Further retreat of the ice margin to the great lakes of Southern Norway. Mainly deposited in Romerike district	
Mytilus- and Cyprina clay	*Mytilus edulis* and *Arctica islandica* *(=Cyprina islandica*)	Improving climatic conditions	Mytilus gravel 9450 ± 250 yr and 9250 ± 250 yr
Older Cardium clay	*Cerastoderma edule* *(=Cardium edule)*		9100 ± 180 yr
Younger Cardium clay	*Cerastoderma edule* *(=Cardium edule)*		
Isocardia clay	*Glossus humanus* *(=Isocardia cor)*	Oslo during shift of the shoreline from 69 to 19 m above present-day sea level. Post glacial climatic optimum	6570 ± 150 yr
Upper Ostrea clay		Disregarded this term in later paper and replaced it with the older part of the Isocardia clay	
Scrobicularia clay	*Scrobicularia plana*	Shift of the shoreline from 19 to 9 (8-10) m above present sea level at Oslo, representing the latest part of the Post Glacial Warm Interval.	1800 ± 150 yr and 660 ± 100 yr

Table 1.2. Foraminiferal zones described by Feyling-Hanssen (1964) with area of deposition, which species of foraminifera are the dominant in each zone and the number of species per 100g sample with some comments. This table is modified from Holtedahl (1960).

Zone	Deposited	Dominant species	Number of species per 100g sample	Comments
A	In or outside the Ra moraines	*Cribroelphidium incertum* (60 – 100%), *Cassidulina crassa* and others	5 – 20	Subzone A_m may correspond to the Ra substage.
B	Inside the Ra moraines superposed on sediments of zone A, further inland resting on ground moraine or bedrock	*Elphidium excavatum subsp. clavatum* (dominates, though less than in A), *Globocassidulina crassa, Stainforthia loeblichi, Nonionellina labradorica*	15 – 25	Subzone B_l may correspond to the Ås-Ski substage.
C	Oldest clay in the district in and near the city of Oslo	Much related to B. Quite common also *Pullenia osloensis* and *Cassidulina teretis*	20	May to some extent correspond to B of the southern area. Assumed to be contemporaneous to the Aker substage by Feyling-Hanssen (1964).
D	Oslo district, most probably also Romerike	Poor fauna. *Elphidium excavatum subsp. clavatum, Globocassidulina crassa, Quinqueloculina stalkeri*	10	Indicate relatively low salinity of the seawater.
E	Both in the outer and inner Oslofjord district	*Elphidium excavatum subsp. clavatum, Cribroelphidium incertum, Cassidulina laevigata, Bulimina marginata*	25	Richer in specimens than previous zones.
F	Occurs as above	*Bulimina marginata* (>50%), *Cribroelphidium incertum, Melonis affinis, Hyalinea baltica*		
G	Occurs as above	Relatively poor fauna dominated by agglutinated forms *Eggerelloides scaber* together with *Ammonia beccarii*		To some extent the clay of this zone (representing a shallow water or even tidal sediment) may be regarded more as a facies unit than a stratigraphical zone. Its foraminifera usually indicate low salinity.

Table 1.3. Holtedahl (1960) correlated Feyling-Hanssen's (1964) foraminiferal zones with Brøgger's (1901) clay deposits. This table shows Feyling-Hanssen's foraminiferal zones correlation with Brøgger's clay deposits.

Foraminifera zonation (Feyling-Hanssen, 1964)	Clay deposits (Brøgger, 1901)
A	Yoldia clay
B	Older and Middle Arca clay
C-D	Younger Arca clay and Portlandia clay
E	Mytilus- and Cyprina clay, probably also Cardium clay or parts of it
F	Isocardia clay, probably also Ostrea clay and parts of Cardium clay
G	Scrobicularia clay

1.3.1 The Ra substage

The Ra substage is identified by moraine ridges on both sides of the outer Oslofjord (Figs. 1.3 and 1.4). Clay deposits of Yoldia clay are found south of this moraine ridge. The Ra moraine is the most predominant moraine complex in the Oslofjord area and can be directly connected with the Skövde moraine and correlated morphologically with deposits in southwestern Sweden (Sørensen, 1979; Andersen et al., 1995). For the most part the Ra moraine consists of two distinct ridges, but in certain places it splits in 3-5 ridges.

Holtedahl (1960) put Brøgger's system of Late- and Post-glacial deposits in the Oslofjord together with Øyen's "Niveau" system, with supposed transgressions (Fig. 1.5). Some radiometric age determinations have been done of the clay deposits shown in Table 1.1. Øyen's interpretation of several transgressions shown to the right in Fig. 1.5 has not been confirmed by later investigations. Neither would such transgression be expected in a district situated centrally in the uplift region where the rate of the landrise was relatively fast. Looking at present day maps it seems that the E6 motorway east of the Oslofjord and E18 west of the Oslofjord are for large parts placed directly on the moraine ridge defining the Ra substage (Fig. 1.3B).

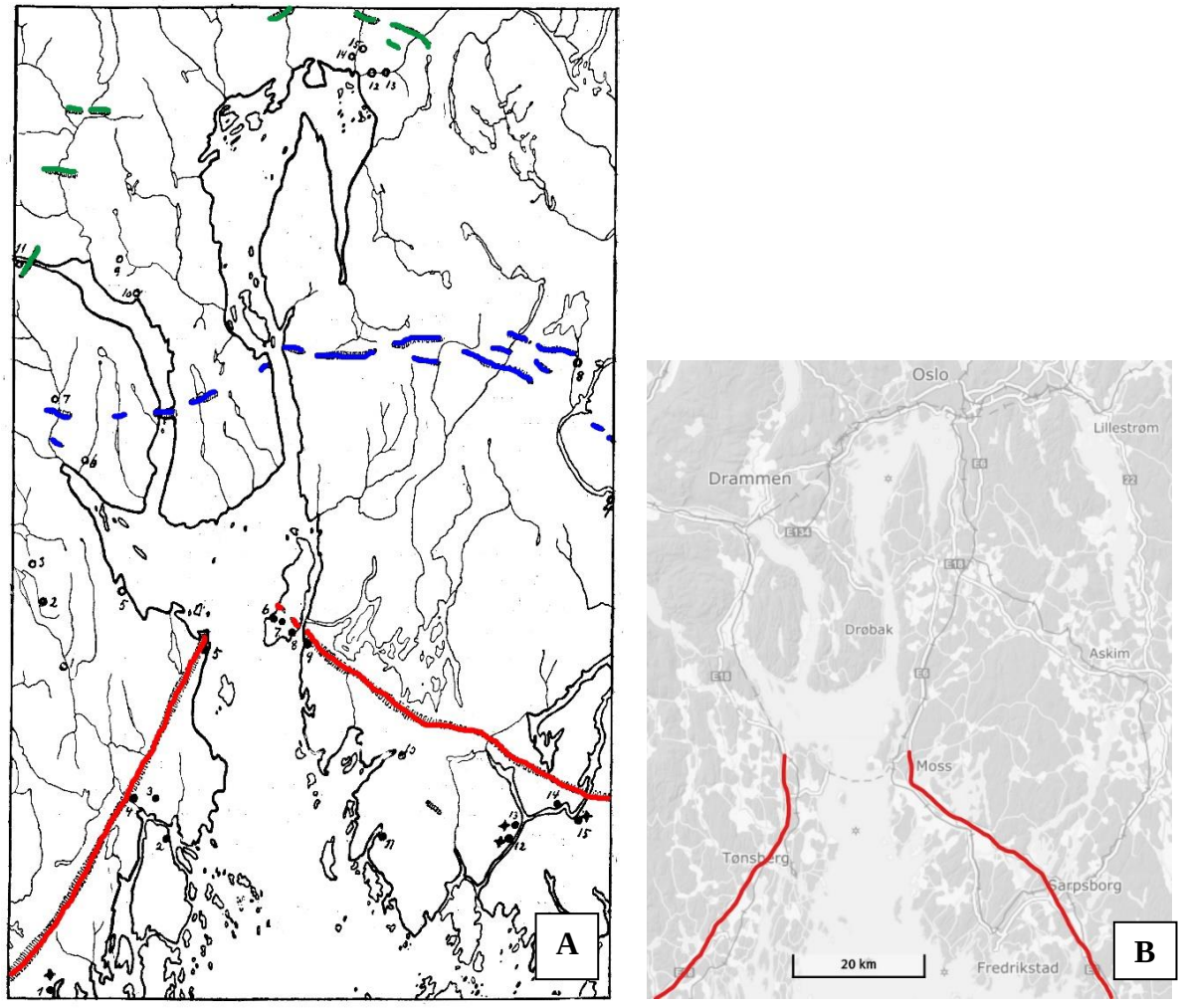

Fig. 1.3 A: an overview of the three moraine ridges, starting in the south with the Ra substage (red), in the middle of the map the Ås-Ski substage (blue) and in the north the Aker substage (green). Modified from Brøgger (1901). B: a modern picture of the same area, showing E6 (east) and E18 (west) are placed approximately on top of the Ra substage with red lines (modified from norgeskart.no).

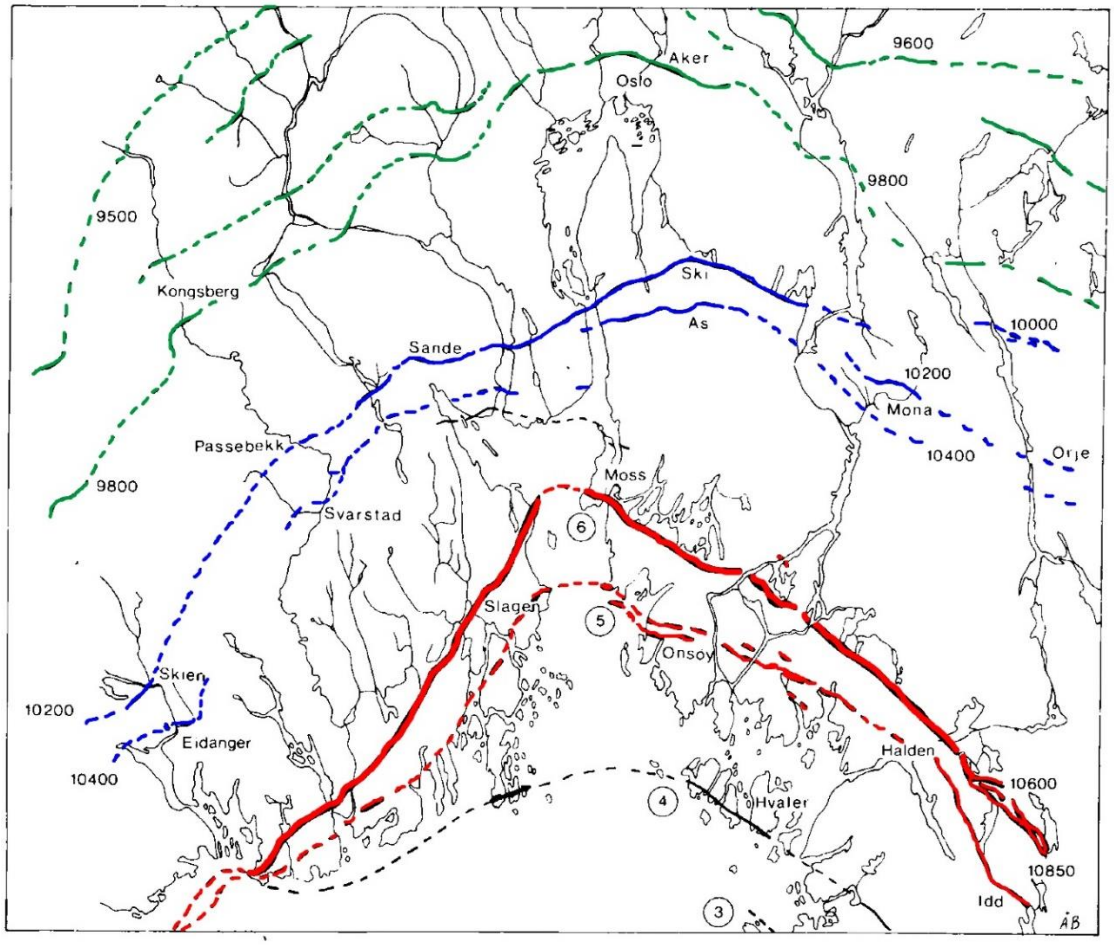

Fig. 1.4. Ra substage (red), Ås-Ski substage (blue) and Aker substage (green). Approximate ages in radiocarbon years. Full lines: ice-marginal deposits. Broken lines: tentative correlation from shoreline diagrams. The moraine ridge farthest south on the map is the Hvaler moraine (black), the oldest recorded moraine ridge in the Oslofjord area. Modified from Sørensen (1979).

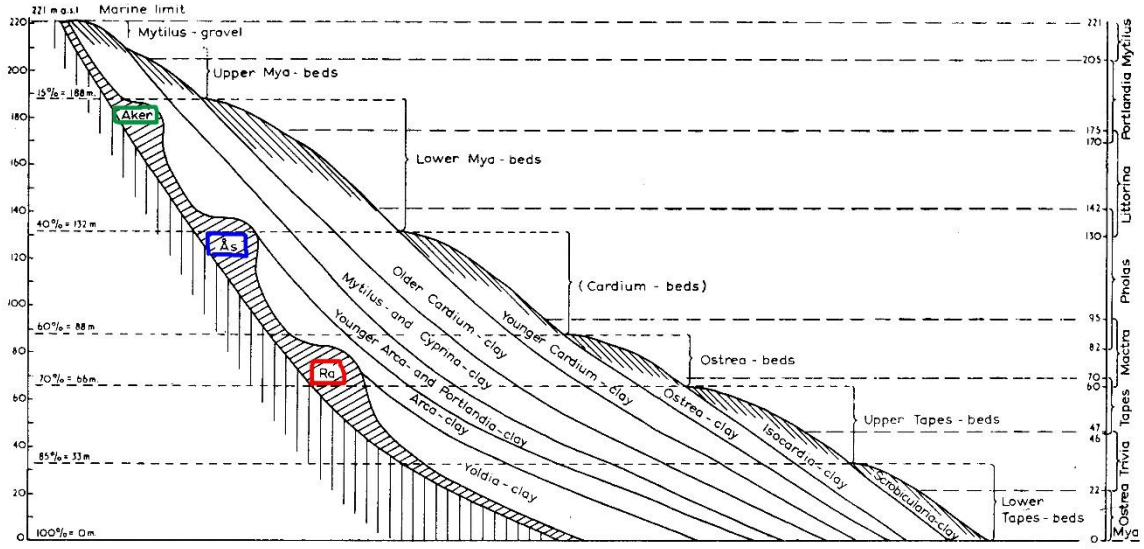

Fig. 1.5. A diagram representing systems worked out by Brøgger and Øyen. Brøgger's system of late- and post-glacial deposits in the inner Oslofjord area is combined with Øyen's "Niveau" system, with supposed transgressions (to the right). Each substage is marked by a colored box, Ra substage (red), the Ås-Ski substage (blue) and the Aker substage (green). Modified from Holtedahl (1960).

1.3.2 The Ås-Ski substage

The Ås-Ski substage, is the second moraine ridge on both sides of the Oslofjord located 20 – 40 km northeast of the Ra moraine (Figs. 1.3 and 1.4; Sørensen, 1979). There is evidence of double moraine ridges or De Geer moraines, moraine landscape consisting of series of separate narrow ridges formed annually and trending parallel to a former ice front, at different locations (Allaby, 2020; Lønne et al. 2001).

The deposition of the Ås-Ski substage reflects the topography at the time, with deep valleys and high hills, the ice stayed in the valleys longer than on the hills and therefore the moraine ridges are not continuous. The moraines are significantly smaller on the west side of the Oslofjord compared to the east side, with small remnants of moraine on the west side and bigger double ridged moraines on the east side. On the west side of the Oslofjord at Storsand (59°39'07.6"N 10°36'10.1"E) there are small remnants of the moraine, while on the east side over Drøbak (59°39'48.0"N 10°37'50.1"E) the moraines are bigger and double ridged. The northernmost moraine ridge in this complex is the Ski moraine and can be followed for more than 60 km. The Ski moraine has been dated to 10,170 ± 190 C^{14} years which gives a median calibrated age of 11,895 cal yr BP (Andersen et al., 1995).

The moraine from both sides of the Oslofjord consists of clay deposits together with a lot of sand and gravel deposits. This clay was not a good preserver of the fauna, the combination of a stand-still of the icecap and large amounts of meltwater accumulating at the front of the icecap resulted in poor conditions for a rich fauna to accumulate (Bøgger, 1901). This zone was difficult for Brøgger and colleagues to investigate due to the low-lying landscape and overlying younger deposits. He was however able to find some locations containing mollusc fauna on the east side of the fjord, along Glomma at Eidsberg approximately 123 – 125m a.s.l. *Bathyarca glacialis* was present with colonies of *Yoldiella lenticula* and *Pseudamussium peslutrae* throughout the terrace and *Anomia ephippium* was found toward the top of the terrace.

The pattern of the moraines at this substage suggests a poorly grounded tidewater glacier with an unstable front, controlled by local topography (Lønne et al. 2001). Some of the ridges show glaciotectonic deformation and interfere with previous ridges, implying that the moraines were formed during a brief ice-front readvance. After the seemingly long standstill of the icecap there was a rapid retreat and melting of the ice.

During deposition of this second moraine ridge and retreat of the icecap Brøgger (1901) concluded the land was sinking instead of rising. Holtedahl (1960) disagreed with this conclusion, Brøgger (1901) judged the sinking of the land based on what he believed was reliable evidence concerning the depth at which various mollusc species live. Today the depth conditions of molluscs are better known and further disproving this conclusion. The deposition of moraines during the Ås-Ski substage was accompanied by glacioisostatic uplift, which induced conditions of a rapid forced regression (Lønne et al., 2001).

1.3.3 The Aker substage

The Aker substage is defined by an oscillation of the ice front, moraines are shown in Figs. 1.3. and 1.4. Brøgger (1901) expected a poor fauna during this substage due to large amounts of freshwater input, meltwater from the ice, and limited supply of saltwater from the sea. Considering his expectations, he found a few locations containing molluscs:

- Galgeberg (Oslo) – *Yoldiella lenticula* and *Similipecten greenlandicus*.
- Hyggen brickwork (Hurumlandet, Asker, Viken) – small molluscs, most likely *Yoldiella lenticula*.
- Spikkestad and Børrestad brickwork (Spikkestad, Asker, Viken) – *Yoldiella lenticula* and *Similipecten greenlandicus*.
    - Øyen also investigated this location and found *Nuculana pernula*, *Chlamys islandica, Musculus discors* and *Ophiura sarsii.*
- The Oslofjord area, directly behind the Ås-Ski moraines – *Yoldiella lenticula* and *Similipecten greenlandicus*.

There were a lot of brickworks around Oslo at the time of Brøgger's investigations that made it easy to get access to deposits from the Aker substage. As the Aker substage consists of younger deposits, Brøgger was able to better investigate at which depth the moraines were most likely deposited. He found the highest marine limit around the Oslofjord being 215 m above present sea-level. All the molluscs defining the Aker substage are possible to find living along the coast today (Brøgger, 1901).

When the crust stopped being pushed down by the icecap, it started rising. The moraines had until this point hindered a connection between the saltwater from the sea and the lakes Mjøsa, Hurdalsvannet, Randsfjorden and others. This raises the question if these at some point have been true fjords, or if the crust started rising before the icecap retreated fully. De Geer also questioned if these lakes were linked to the sea at this time (Brøgger, 1901).

1.3.4 The Preboreal Oscillation

Terrestrial records of northwest Europe have shown a two-step warming of sea surface temperatures around the Younger Dryas – Preboreal transition dated respectively to 10,200 – 10,000 and 9,700 – 9,500 ^{14}C yr BP (Hald & Hagen, 1998). Between these two warming steps there was a short time interval of no temperature rise or cooling. This period was climatically unstable and is termed the Preboreal oscillation (PBO). It appears to have been a synchronous event in the Northern Hemisphere (Björck et al., 1996). Evidence from lacustrine sediments, tree-rings and glacial records also show evidence of a PBO (Björck et al., 1997). It is characterized by cooling and humid conditions throughout northwest and central Europe. Main driving forces of the deglacial climate oscillations are thermohaline circulation and ocean ventilation rates (Björck et al., 1997). Previous reports of the PBO in lacustrine sediments include detailed pollen studies of Holocene sediments from central Europe, northern Germany, Great Britain, Denmark and the Netherlands (Björck et al., 1997). Bjørklund et al. (2019) show a ca. 2 °C drop in temperature around the presumed PBO in northern Norway. Based on an OxCal age model they predicted an age of 11,390 – 11,520 cal yr BP. Behre (1978), discussed in Björck (1997), examined European Preboreal pollen data, ^{14}C dates and sedimentation rates and concluded that the cooling started some hundred years after the end of the Younger Dryas and placed the PBO between ca. 10,000 – 9,600 yr B.P. Björck et al. (1996) studied three sets of closely AMS dated terrestrial macrofossils in lake sediments and pollen stratigraphical correlations. With this they found that the cooling began when the 10,000 – 9,900 ^{14}C plateau ended, i.e. 250 yr after the end of the Younger Dryas. Björck et al. (1996) pointed out the rising δ^{14}C values during the PBO make it difficult to assign it a well-defined ^{14}C age: it covers a time period of 100 – 150 calendar years corresponding to 300 – 400 ^{14}C years (Björk et al. 1997). It is suggested, based on box-model calculations considering the rapid shift in atmospheric ^{14}C, that the cooling during the PBO was caused by a large freshwater input of the North Atlantic heat conveyor (Hald & Hagen, 1998). The most precise dating of the PBO was done by Rasmussen et al. (2007) through ice-core dating, giving an age of 11,400 – 11,500 cal yr BP.

2 Materials and methods

All localities sampled during a field trip are presented in Fig. 1.2. The historical locality MG1 (marine limit + number of the locality) was visited, a sample from this locality was collected ca. 221m a.s.l. and analyzed in the lab at the Natural History Museum, Økern, together with the three samples presented below. Fig. 2.1B shows the locality was overgrown by trees and shrubs, making the sampling somewhat difficult. To make sure the marine sediments were collected from this locality, a small hole was dug in the hillside to surpass the sediments placed there by human activity, erosion debris from Grefsenkollen and the area surrounding the locality. This contrasts the open landscape during Brøgger's (1901) investigation shown in Fig. 2.1A.

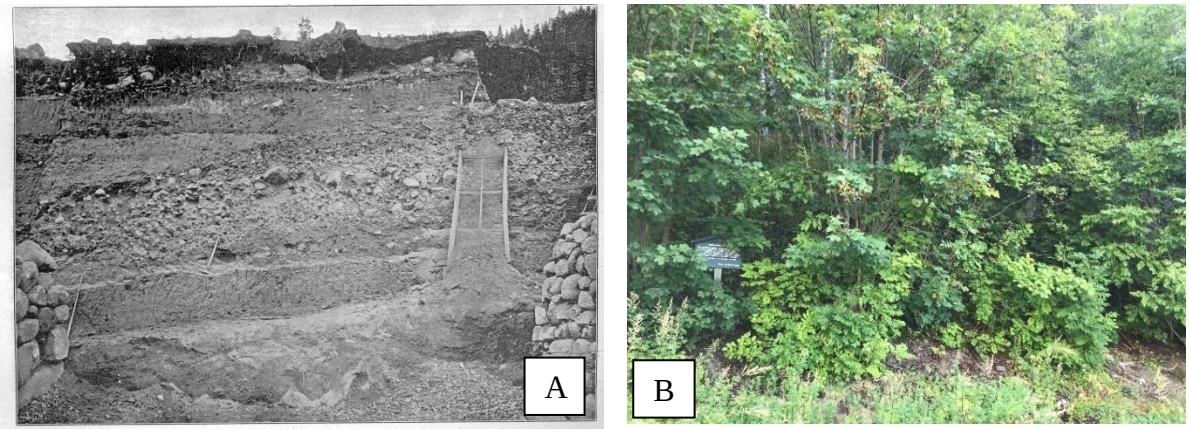

Fig. 2.1. Photos comparing the Grefsen location (MG1). A: an old photo from Brøgger (1901) with great exposure of the location. B: Picture of the same location taken in 2019, with a sign for scale.

Walking along the S-W side of Grefsenkollen, location MG2 was found (Fig. 1.2). It is located behind a house on Friggs vei in front of Grefsenkollen ca. 226m a.s.l. It seemed to be a terrace covered with trees and shrubs, here a sample was taken in the same manner as for MG1. This was not a historical locality reported by Brøgger (1901). MG3 is located behind a house on Ymers vei ca. 226m a.s.l. Although it was in a residential area and therefore heavily modified, it resembled a terrace. The last location found during the field trip was MG4. This was another historical locality where Brøgger (1901) reported having found macrofossils. MG4 is located on a hill S-W of Oslo Østre Skytterlag ca. 217m a.s.l. Again, the landscape was modified by human activity and the sample taken from this locality did not contain any macro- or microfossils. In addition to the four field samples collected, a sample from Sognsvann was studied. This sample was from the collection of the Natural History Museum

and collected by Johannes Dons in 1940 from the lower part of a shell bed in Sandås near Sognsvann ca. 192m a.s.l. (Fig. 2.2).

From the Sognsvann locality one sample contained a sandy matrix with *Mytilus edulis* specimen attached to the matrix (Fig. 2.3). This box was used for wet sieving of the sediment, and ostracods and foraminifera were found. Another box from the same locality contained a collection of macrofossils including *Mytilus edulis* used for LA-ICPMS analyses (Fig. 2.2). A small piece of another *Mytilus edulis* shell from this box was selected and sent for ^{14}C dating at the University of Lund, Sweden.

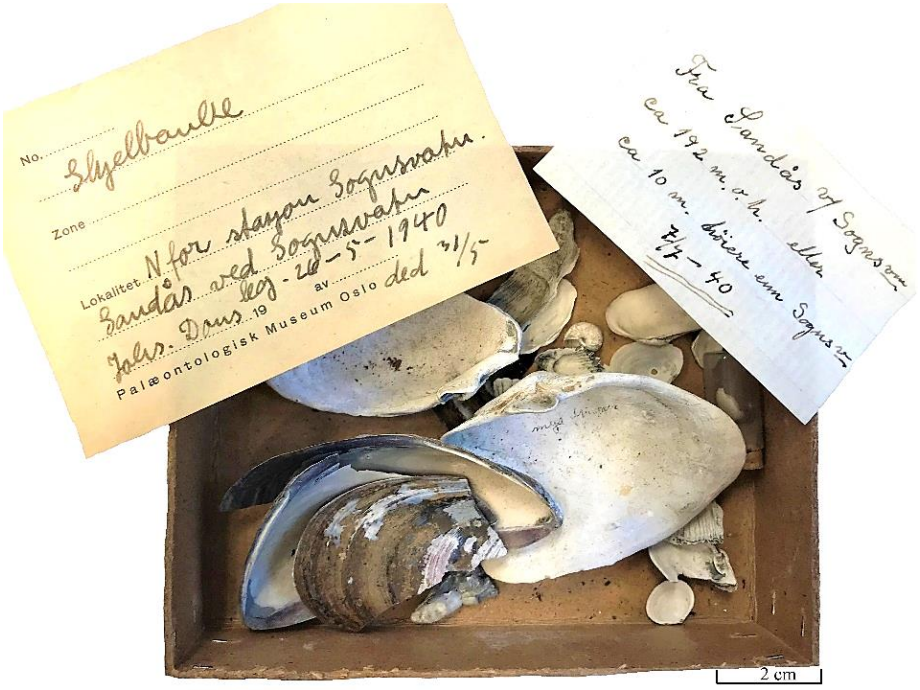

Fig. 2.2. Sample from the Sognsvann location, from the collection of the NHM, museum accession number PMO 3520A.

Fig. 2.3. Sample from the Sognsvann location. Sediment tightly packed with micro- and macrofossils attached to the sediment. From the collection of the NHM, PMO 3520B.

Skådalen is another historical locality mentioned by Brøgger (1901). Some samples from the collection of the Natural History Museum containing sediments and fossils from this locality were also analyzed. One sample containing abundant *Balanus* sp. collected ca. 221m a.s.l. and previously radiocarbon dated in 1959 was sampled for a new radiocarbon dating (Fig. 2.4).

Fig. 2.4. Sample of *Balanus sp.* from the Skådalen location. From the collection of the NHM, PMO3502.

Another sample from the Skådalen location from the Natural History Museum collection (Fig. 2.5) was also included in the study. This contained a rock with macrofossils (*Balanus)* and some shell fragments together with a shell of *Mytilus edulis* used for LA-ICPMS analysis, and $\delta^{18}O$ and $\delta^{13}C$ analyses. A fragment from a *Mytilus edulis* shell was also selected for radiocarbon dating. The sample was collected ca. 221m a.s.l.

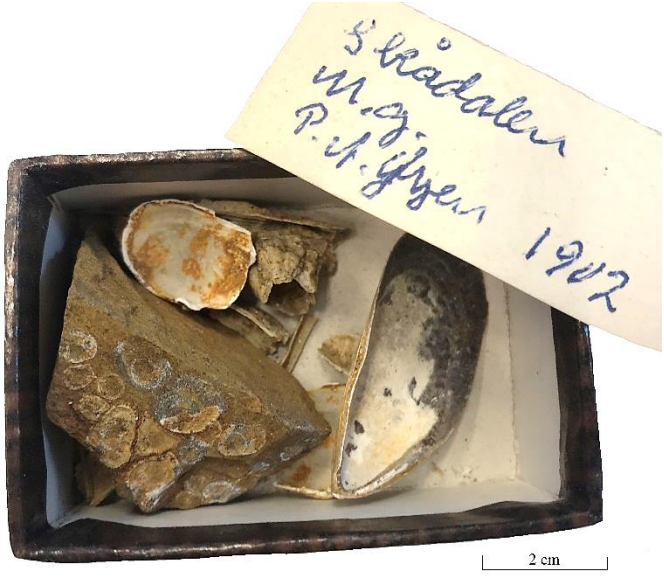

Fig. 2.5. Sample from the Skådalen location. A rock with macrofossils, some shell fragments and a shell of *Mytilus edulis*. From the collection of the NHM, PMO 3500.

Some material from Vardeåsen, Nesodden was also analyzed. The sample was collected by Jan Kornstad ca. 176m a.s.l. He had collected a lot of sediments containing many different fossil species. *Mya truncata* was selected for radiocarbon dating.

Fig. 2.6. A representation of the fauna from Vardeåsen, Nesodden. Collected by Jan Kornstad ca. 176m a.s.l.

2.1 Abbreviations

Table 2.1 is an overview of all the abbreviations used in this thesis.

Table 2.1 A table of abbreviations.

Abbreviation	Explanation
cal yr BP	Calibrated Years Before Present (radiocarbon years before 1950)
a.s.l.	Above sea level
PBO	Preboreal Oscillation
MG	Marin grense (Marine limit)
LA-ICPMS	Laser Ablation-Inductively Coupled Plasma-Mass Spectrometry
SEM	Scanning Electron Microscopy
BSE	Backscattered Electrons
AMS	Accelerator Mass Spectrometry
PSU	Practical salinity units
DIC	Dissolved inorganic carbon
VPBD	Vienna Pee Dee Belemnite
VSMOW	Vienna Standard Mean Ocean Water

2.2 Laser Ablation-Inductively Coupled Plasma-Mass Spectrometry (LA-ICPMS)

Laser Ablation-Inductively Coupled Plasma-Mass Spectrometry (LA-ICPMS) makes it possible to analyze fast growing animals, like *Mytilus edulis* and their seasonal growth patterns (Putten et al. 2000). The chemical archives of the shells can record seasonal changes and variations in environmental parameters. The precision of the laser makes it possible to measure with high sample density along very narrow shell profiles and is therefore ideal for detecting small changes in element concentration.

Before performing the LA-ICPMS analysis the shell was sawed in half and mounted in epoxy, then polished and trimmed to fit in the instrument. The quadrupole is a Bruker Aurora Elite which is connected to a Cetac LSX-213 G2+ laser. The calculations were done in Glitter and standardized with NIST-610 (Jochum et al., 2011) and CaO as internal standard. Each analysis lasted 55 seconds, 15 seconds background measurement and 40 seconds sample measurement. When measuring the standard (610) a laser diameter of 100 microns was used and for the samples a laser diameter of 50 microns was used. Pulse frequency for both was 10 Hz. The laser used does not measure fluence.

LA-ICPMS analysis was performed on two *Mytilus edulis* shells, one from the Skådalen locality and one from the Sognsvann locality. The results from this analysis are to be found in Appendix 1 – 4.

2.2.1 PPM to µmol/mol

For comparison with Gillikin et al. (2006) ppm values of Ba and Ca needed to be converted to:

$$\frac{\mu mol\ Ba}{mol\ Ca}$$

In converting ppm to mol, first multiply the results with 10^6 and divide with the atomic weight of each element and assuming 1g of shell was analyzed for each sample:

$$\frac{\mu mol\ Ba}{mol\ Ca} = \frac{10^6 \times mol\ Ba}{mol\ Ca} = \frac{10^6 \times \left(\frac{ppm\ Ba}{137} \times 10^6\right)}{\frac{ppm\ Ca}{40} \times 10^6}$$

$$= \frac{10^6 \times ppm\ Ba}{ppm\ Ca} \times \frac{40}{137}$$

The results have normalized Ca values of 400000 ppm and therefore insert this number:

$$\frac{\mu mol\ Ba}{mol\ Ca} = \frac{10^6 \times ppm\ Ba}{400000} \times \frac{40}{137} = ppm\ Ba \times \left(\frac{10^6}{400000} \times \frac{40}{137}\right)$$

Ending up with this equation:

$$\frac{\mu mol\ Ba}{mol\ Ca} \approx ppm\ Ba \times 0.73$$

2.3 Isotope analysis

Small chips were broken off the edge of the cut shell with pliers. The chips were analyzed for $\delta^{18}O$ and $\delta^{13}C$ at FARLAB, University of Bergen, with a Thermo Scientific MAT253 mass spectrometer coupled to a Kiel IV online carbonate device. External precision (1-sigma of >240 standard runs over the same period) was 0.03‰ for C and 0.06‰ for O isotopes. Results are reported in permil VPDB.

Ten samples were broken off the edge of the cut shell with pliers (Fig. 2.8). Doing this by hand was not as precise as the LA-ICPMS analysis. Using a drill in the existing holes from the LA-ICPMS analysis performed on the other half of the shell, like Putten et al. (2000), would have given a higher resolution of the $\delta^{18}O$ curve and a better foundation for comparison with the Ba curve.

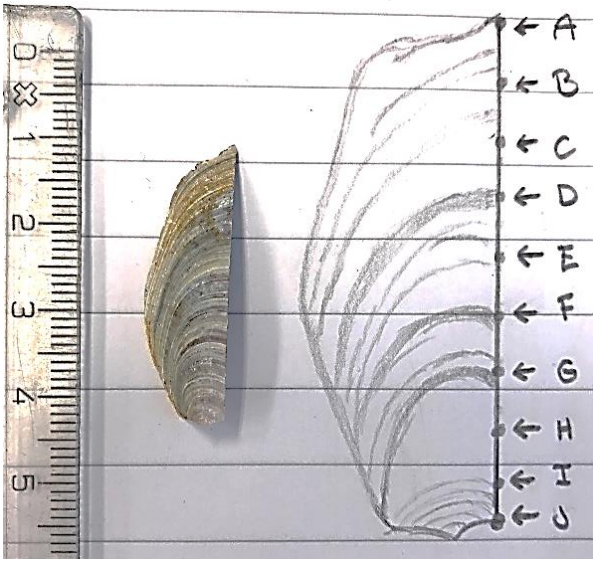

Fig. 2.8. Picture of *Mytilus edulis* shell from Skådalen before sampling for oxygen isotope analysis. Sketch to the right shows where the samples were taken along the shell.

2.4 Scanning Electron Microscopy (SEM)

Scanning electron microscopy (SEM) can image and analyze bulk specimens (Reimer, 2013, p. 1). Electrons from a cathode are accelerated through a voltage difference between cathode and anode that may be as low as 0.1 kV or as high as 50 kV (Reimer, 2013, p. 8). In this case backscattered electrons (BSE) were used to create images.

SEM imaging was done on ostracods found in the sample from Sognsvann. The ostracods were found in fraction 250 – 500 µm and 24 ostracods were picked. First all the ostracods were glued to a paper lined tray and imaged from the outside. I proceeded to turn all of them and glued them to the tray, so the inside of all the ostracods could be imaged. Some of the ostracods had sand and particulates inside their shells, a brush was used with water to remove the particulates from the inside, to make sure the muscle attachments would be visible and make species identification easier. However, all the particulates were not removed inside all the 24 shells. The 19th ostracod was destroyed when it was turned due to a weakness in its shell. The muscle attachment was lost when it broke. The imaging was done at the lab of the Natural History Museum, Økern.

2.5 Radiocarbon dating

Ca. 15 mg of shell material was sampled from each of the four shells and sent to the for ^{14}C dating at a laboratory at the University of Lund, Sweden. The calculation used a half time of 5568 years and the ages are reported as ^{14}C years B.P. (1950).

Age calibration used Calib version 7.1 (Stuiver et al. 2020, calib.org) with the Marine13 marine reservoir correction. A delta R value of 0 years was used, given the uncertainty in local reservoir age in the earliest Holocene. This uncertainty should be kept in mind when interpreting the calibrated ages.

2.6 Field samples

Four different localities were sampled in the field (Fig. 1.2). They were wet sieved and separated into fractions (Fig. 2.9). Looking at the different fractions no foraminifera were present in any of the samples.

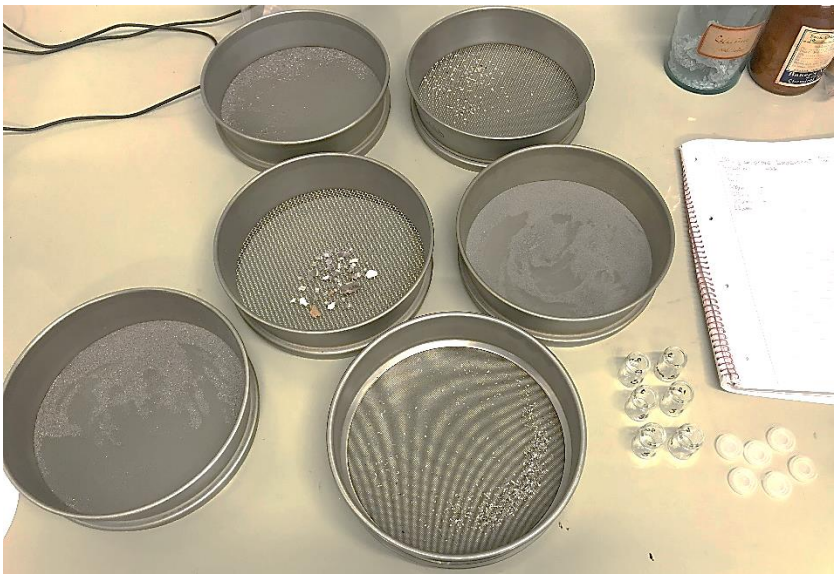

Fig. 2.9. Wet sieving of Sognsvann sample. A4 notebook for scale.

Further, one sample from the collection of the Natural History Museum (the Sognsvann sample) was sieved. Looking in the microscope at fraction 250 – 500 µm a lot of ostracods and some foraminifera were observed (*Stainforthia* sp. and *Elphidium* sp.), along with sand and some terrestrial plant material. I proceeded picking out ostracods and foraminifera from the sample for further analyses.

2.7 Pictures

In photographing different samples and shells for this thesis an iPhone 7 was mainly used, which has a 12-megapixel camera. CT scanning with the Nikon Metrology XT H 225 instrument at NHM was also used, in order to bring out subtle growth increments. Cut shells mounted in epoxy were scanned on a flatbed scanner. Images used in this thesis were edited using Adobe Photoshop.

3 Results

3.1 Laser Ablation-Inductively Coupled Plasma-Mass Spectrometry (LA-ICPMS)

3.1.1 Skådalen

An LAICP-MS analysis was performed on a *Mytilus edulis* shell from the Skådalen locality. Fig. 3.1 shows the sample location along the shell with yellow dots.

Values of Ba are high close to the umbo, up to ca. 5mm, then it flattens out until a peak at 20mm (Fig. 3.2). This is the highest peak with a value of 171.18 ppm at 21mm. Further it dramatically drops before a smaller peak at 26.5mm. There is a possible peak at 30.5mm, though not as predominant as the first peaks. At 38mm there is evidence of the last peak in Ba.

Sr shows no clear trends along the shell (Fig. 3.2). There are some fluctuations in Sr between the Ba peaks, but no visible trend throughout the shell. Mg, like Sr, does not show any clear trends throughout the shell. At 26.5mm all the elements have a visible peak at the same time, but this is not evident in any other part of the diagram.

Fig. 3.1. Scanned picture of *Mytilus edulis* shell from Skådalen after LA-ICPMS analyses were performed. Yellow dots show each laser ablation point alongside the shell. The shell is ca. 4.5 cm in length.

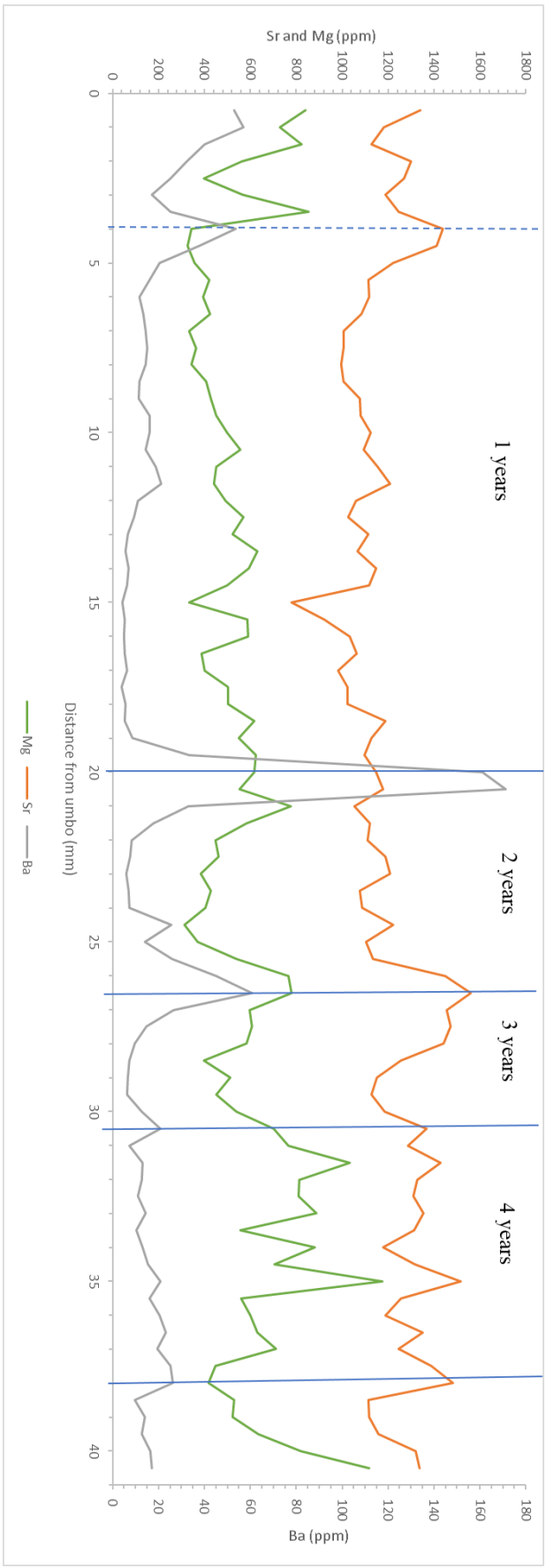

Fig. 3.2. Concentrations of Sr (red), Mg (green) and Ba (gray) along *Mytilus edulis* shell from the Skådalen location. Blue lines indicating peaks in Ba. All the values can be found in Appendix 1 and 2.

For comparison with Gillikin et al. (2006) the values of Ba/Ca were converted from ppm to µmol/mol using the equation from chapter 2.2.1 (Fig. 3.3).

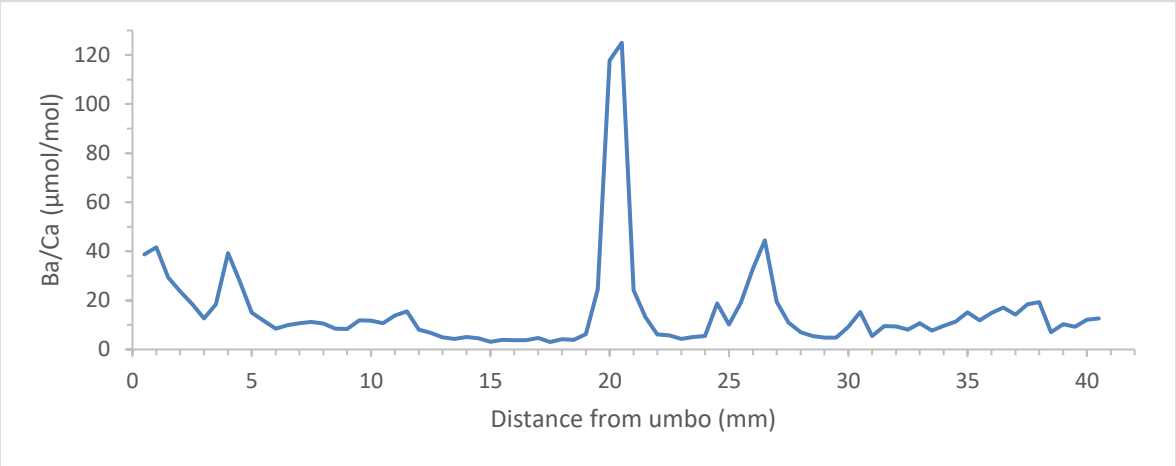

Fig. 3.3. Diagram of Ba/Ca (µmol/mol) along *Mytilus edulis* shell from the Skådalen locality starting at umbo. Table of values in Appendix 2.

3.1.2 Sognsvann

An LAICP-MS analysis was performed on a *Mytilus edulis* shell from the Sognsvann location. Fig. 3.4 shows the sample locations along the shell with yellow dots.

Ba has its first peak from the umbo up to ca. 10mm, shown with blue line in Fig. 3.5. Further Ba peaks at 28mm, 36mm, 47.5mm, 62mm, 67mm and 69mm, all marked with blue lines in Fig. 3.5. Sr shows no apparent trends, though it seems to correlate with Ba, this was not evident in the Skådalen shell. In this shell the analysis was done on both the aragonite layer and the calcite layer of the shell (Fig. 3.4). This could make interpreting the diagram somewhat difficult. Mg values seem to be very low from umbo to 55mm, where the values start to rise. It seems that Mg, Sr and Ba have peaks at the same time at 67mm and 69mm.

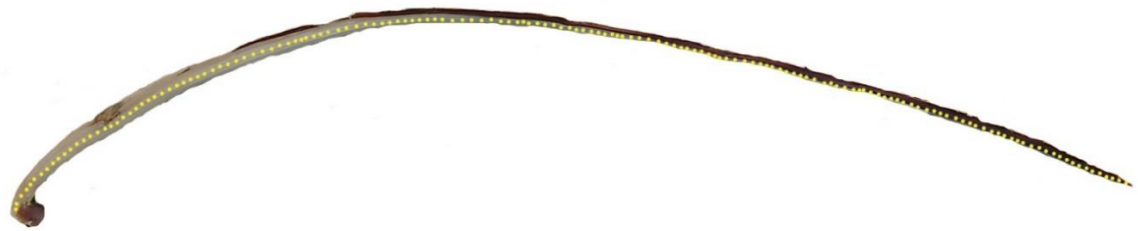

Fig. 3.4. Scanned picture of *Mytilus edulis* shell from Sognsvann after LA-ICPMS analyses was performed. Yellow dots show each laser ablation point along the shell. The shell is ca. 7.8 cm in length.

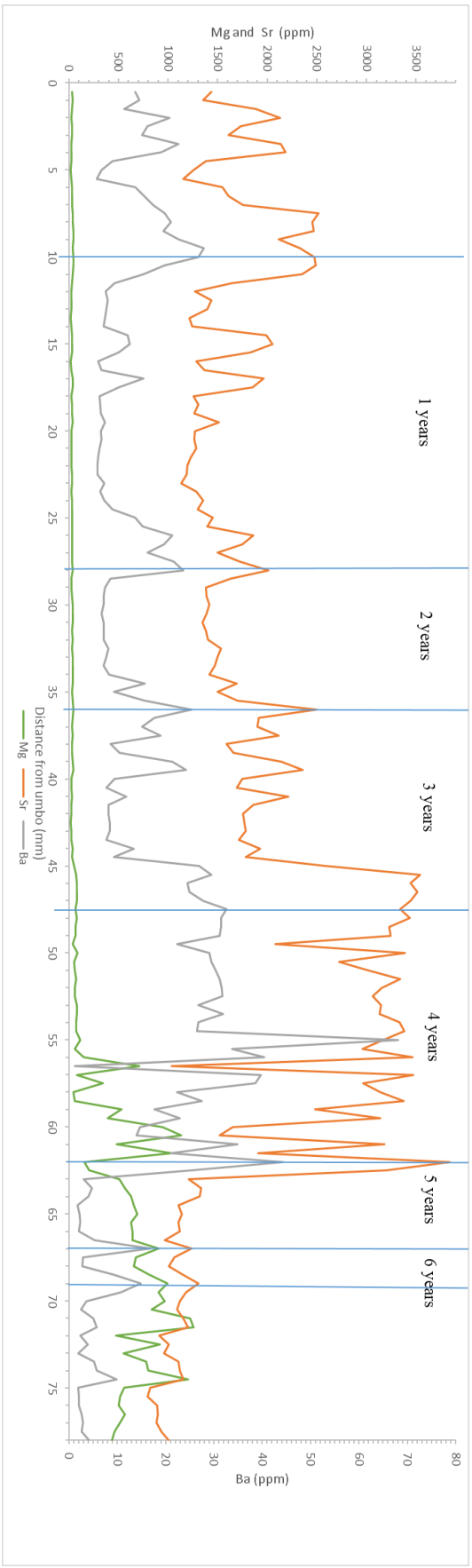

Fig. 3.5. Concentration of Sr (red), Mg (green) and Ba (gray) along *Mytilus edulis* shell from the Sognsvann location starting at umbo. Blue lines indicating peaks in Ba. Table of values in Appendix 3 and 4.

For comparison with Gillikin et al. (2006) the values of Ba/Ca were converted from ppm to µmol/mol using the equation from chapter 2.2.1 (Fig. 3.6).

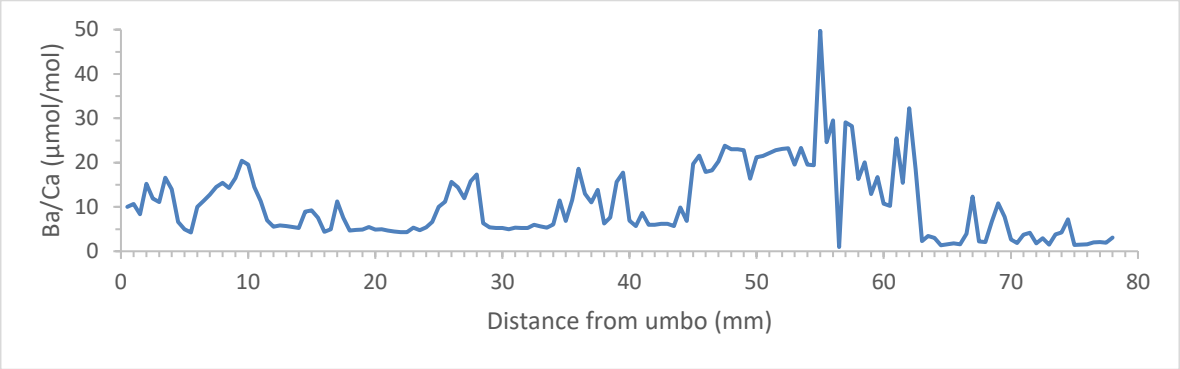

Fig. 3.6. Diagram of Ba/Ca (µmol/mol), calculated using equation in method chapter, along *Mytilus edulis* shell from the Sognsvann locality starting at umbo. Table of values in Appendix 4.

3.2 CT pictures of *M. edulis* shells

Growth zones shown on the CT pictures could indicate the Skådalen shell is 4 – 5 years old (Fig. 3.7), while the Sognsvann shell is 6 years old (Fig. 3.8).

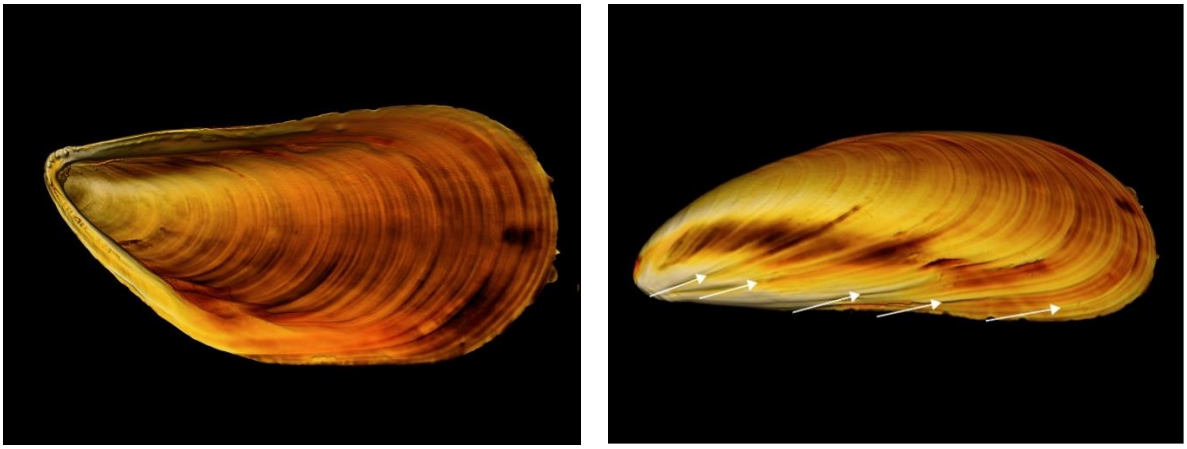

Fig. 3.7. CT picture of *Mytilus edulis* shell used for LA-ICPMS and oxygen isotope analyses from Skådalen locality. Shell is ca. 4.5 cm in length, with arrows showing growth rings.

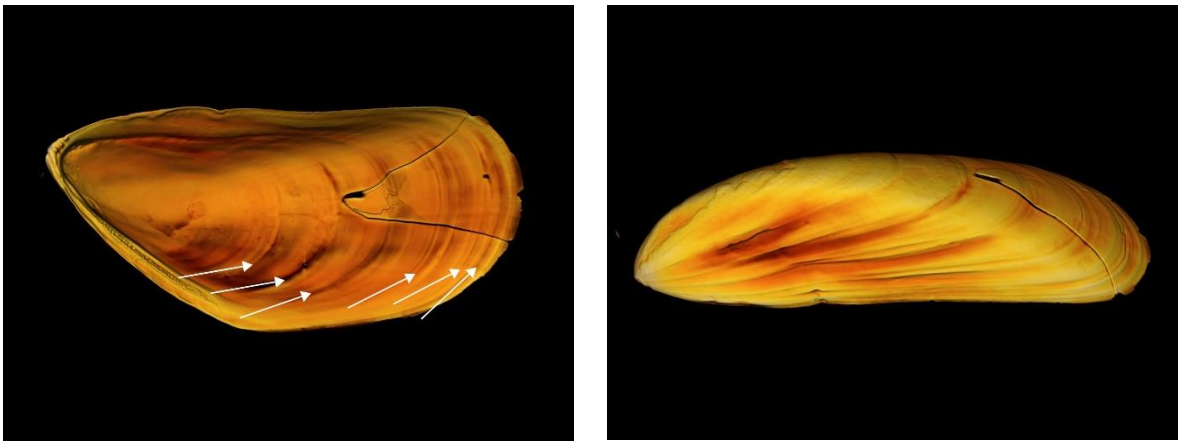

Fig. 3.8. CT picture of *Mytilus edulis* shell used for LA-ICPMS from Sognsvann locality. Shell is ca. 7.8 cm in length, with arrows showing growth rings.

3.2.1 Bivalve growth

Growth rings in bivalve shells have in several cases been shown to be formed annually (review in Seed, 1976). The rings can be laid down when the shell growth is disturbed, due to adverse temperature conditions, reproduction or variations in food availability. Generally, the rings seem to be most distinct if annual growth rate shows pronounced variations. Sometimes several rings are formed annually (Seed, 1976). Since *Mytilus edulis* in the Northern Baltic seems to have only one reproductive period, immediately following the winter growth minimum, Kautsky (1982) assumed in his study that the growth rings were formed only once

per year. This view was followed in this thesis and identify 4 – 5 annual growth rings on the shell of *Mytilus edulis* from the Skådalen location and 6 annual growth rings on the shell of *Mytilus edulis* from the Sognsvann location (Fig. 3.7 and 3.8).

3.3 Radiocarbon dating

Table 3.1 shows new radiocarbon datings, using calib.org with MARINE13, a webpage that can be used for calibrating radiocarbon ages. These are the most recent datings for each of the localities and shows ages older than previously reported from near the marine limit in the Oslo area.

Table 3.1. Results radiocarbon dating: Location of each sample is shown in Fig. 1.2. The genus dated is shown in the Taxon column, with the uncalibrated radiocarbon age and error under ^{14}C age ± 1σ. The calibrated age range with 95% confidence interval is shown under cal BP (95%), and the calibrated median age of each location under Median cal BP. All the calibrated radiocarbon ages have had 1950 years added to the values extracted from calib.org.

Location	Taxon	^{14}C age ± 1σ	cal BP (95%)	Median cal BP
Nesodden	*Mya*	9915 ± 50	11,057 – 10,704	10,877
Skådalen	*Balanus*	6265 ± 40	6836 – 6619	6717
Skådalen	*Mytilus*	10,260 ± 70	11,585 – 11,102	11,262
Sognsvann	*Mytilus*	10,150 ± 70	11,297 – 10,955	11,150

3.4 $\delta^{18}O$ and $\delta^{13}C$

Results from the oxygen isotope analysis are shown in Table 3.2 and Appendix 5.

Table 3.2 Oxygen isotope analysis: Samples were taken along the shell of *Mytilus edulis* from the Skådalen location (Fig. 2.8). An approximate distance from umbo is given for each sample in the column, Distance from umbo (mm). The results for $\delta^{13}C$ (VPDB) and $\delta^{18}O$ (VPDB) are also shown.

Sample	Distance from umbo (mm)	$\delta^{13}C$ (VPDB)	$\delta^{18}O$ (VPDB)
J	3	-2.16	-4.43
I	6	-1.31	-1.55
H	10	-1.11	-3.27
G	13	-0.83	-0.30
F	17	-0.64	-3.05
E	20	-0.36	-1.52
D	23	-1.06	-1.92
C	27	-0.83	-0.89
B	30	0.21	-3.23
A	34	-2.01	-3.87

Looking at the diagram of the oxygen isotopes of the *Mytilus edulis* shell from the Skådalen location (Fig. 3.10), values of $\delta^{18}O$ are plotted against approximate distance from umbo. There are four negative peaks present, at 3mm (-4.43‰ VPDB), 10mm (-3.27‰ VPDB), 17mm (-3.05‰ VPDB) and 30mm (-3.87‰ VPDB) with declining values until the end of the shell at 34mm. Carbon isotope ratios are shown in Fig. 3.11.

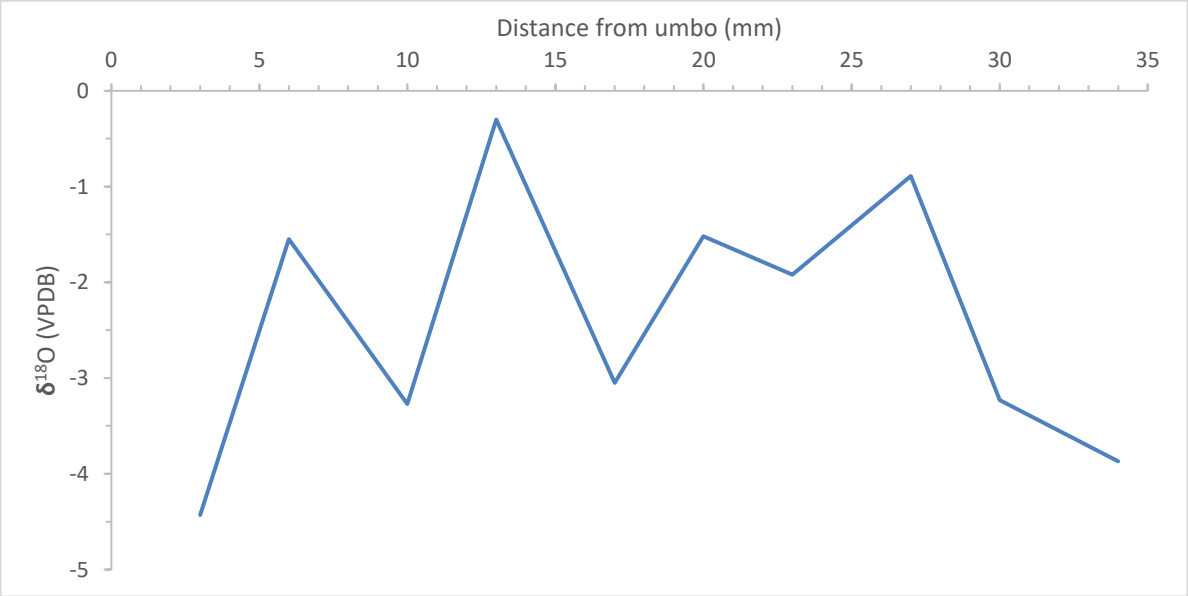

Fig. 3.10. Diagram showing oxygen isotopes of *Mytilus edulis* shell from the Skådalen location in relation to distance from umbo. Values in Appendix 5.

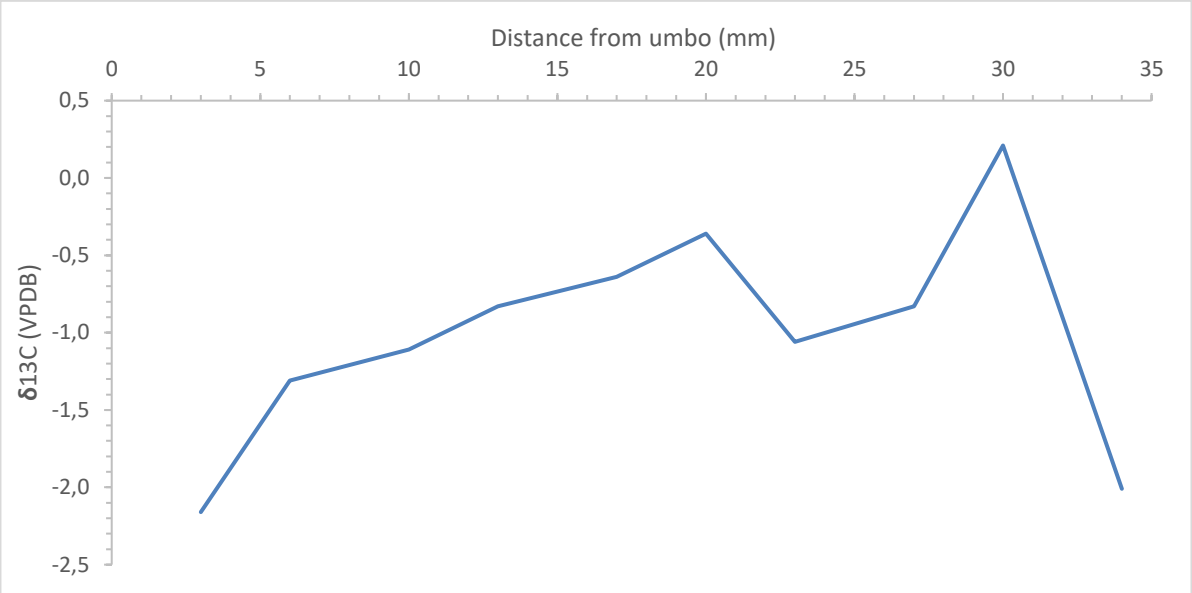

Fig. 3.11. Diagram showing carbon isotopes of *Mytilus edulis* shell from the Skådalen location in relation to distance from umbo. Values in Appendix 5.

3.5 Field samples

Table 3.3 show the result of wet sieving the four samples collected during the field trip, and the sample from the Sognsvann location from the collection of the Natural History Museum. All the locations except from the Sognsvann location are marked on the map in Fig. 1.2. The sample from Sognsvann was not weighed before wet sieving and a lot of the clay fraction was lost during sieving. The Sognsvann location has not been placed on the map because the exact location where the sampling took place is not known.

Table 3.3 Field samples: The localities of samples collected from MG1 – MG4 are shown in Fig. 1.2. The Sognsvann sample was taken from a box from the collection of the Natural History Museum. All the samples (except of Sognsvann) were weighed before wet sieving (the Sognsvann sample could not be analyzed again because of the Covid-19 lockout). After the different fractions were dry, they were weighed again, as shown in the table. The weight of all the fractions after wet sieving were combined in the last column to get an indication of the clay fraction lost during wet sieving.

Sample	Weight before sieving (g)	4 mm	2 mm	1 mm	500 µm	250 µm	125 µm	63 µm	25 µm	Weight after sieving (g)
MG1	76.8	7.48	3.58	5.44	7.87	9.67	17.52	14.94	4.15	70.65
MG2	70.37	5.92	8.93	10.3	12.8	11.44	9.64	6.35	1.69	67.07
MG3	48.54	1.99	1.63	1	2.78	6.97	5.18	5.99	6.45	31.99
MG4	88.1	10.67	1.48	1.86	2.94	5.38	6.64	2.76	3.25	34.98
Sognsvann			1.71	0.69	1.04	3.43	10.5	13.74		31.11

3.6 Ostracods

Figs. 3.12 – 3.15 show SEM imaging of ostracods found in the Sognsvann sample. The figures show the outside and inside of each specimen. At least three species are identified; *Cythere lutea* (Fig. 3.12), *Sarsicytheridea bradii* (Fig. 3.13), *Sarsicytheridea punctillata* (Fig. 3.14) and unidentified ostracod species (Figs. 3.12, 3.13, 3.14, 3.15).

Ostracods are widely distributed marine and freshwater crustaceans, their entire body is enclosed in a rounded or elliptical, bivalve, shell consisting of calcium carbonate (Allaby, 2009). The muscle has a cluster of transverse adductor muscle fibers to close the valves, while the animal lives in the center of each valve. Its head accounts for most of its body, because the trunk appendages usually are reduced to two pairs and there is no external segment to the trunk. There is a wide range of feeding types amongst ostracods. They include filter feeders, carnivores, herbivores and scavengers. The sexes are separate for this class and parthenogenesis is common amongst freshwater forms. There are more than 2000 living species and 10 000 fossil species ranging from the early Cambrian to the present.

Ostracods can live in a variety of salinity. The identified species below can be placed in three different groups. They are divided based on the different salinity categories each ostracod species prefer: Oligohaline, which is a category with low salinity, brackish water (>0.5 – 5‰); Mesohaline, a category with relatively low salinity, brackish water (>5 - 18‰); Polyhaline, a category with moderately saline water, but not reaching sea water salinity (>18 - 30‰); Euhaline, a category with fully saline water, sea water (>30‰) (Stepanova et al., 2019).

Cythere lutea – Salinity: 5 - > 30 ‰. Group 4, Meso-, poly, euhaline, shallow-water to deep, open sea taxa (Stepanova et al., 2019).

Sarsicytheridea bradii – Salinity: 6.5 to > 30 ‰. Group 4, Meso-, poly, euhaline, shallow-water to deep, open sea taxa (Stepanova et al., 2019).

Sarsicytheridea punctillata – Salinity: 3.8 to > 30 ‰. Group 2, Oligo-, meso-, poly-, euhaline, very shallow and shallow-water coastal and open sea taxa (Stepanova et al., 2019).

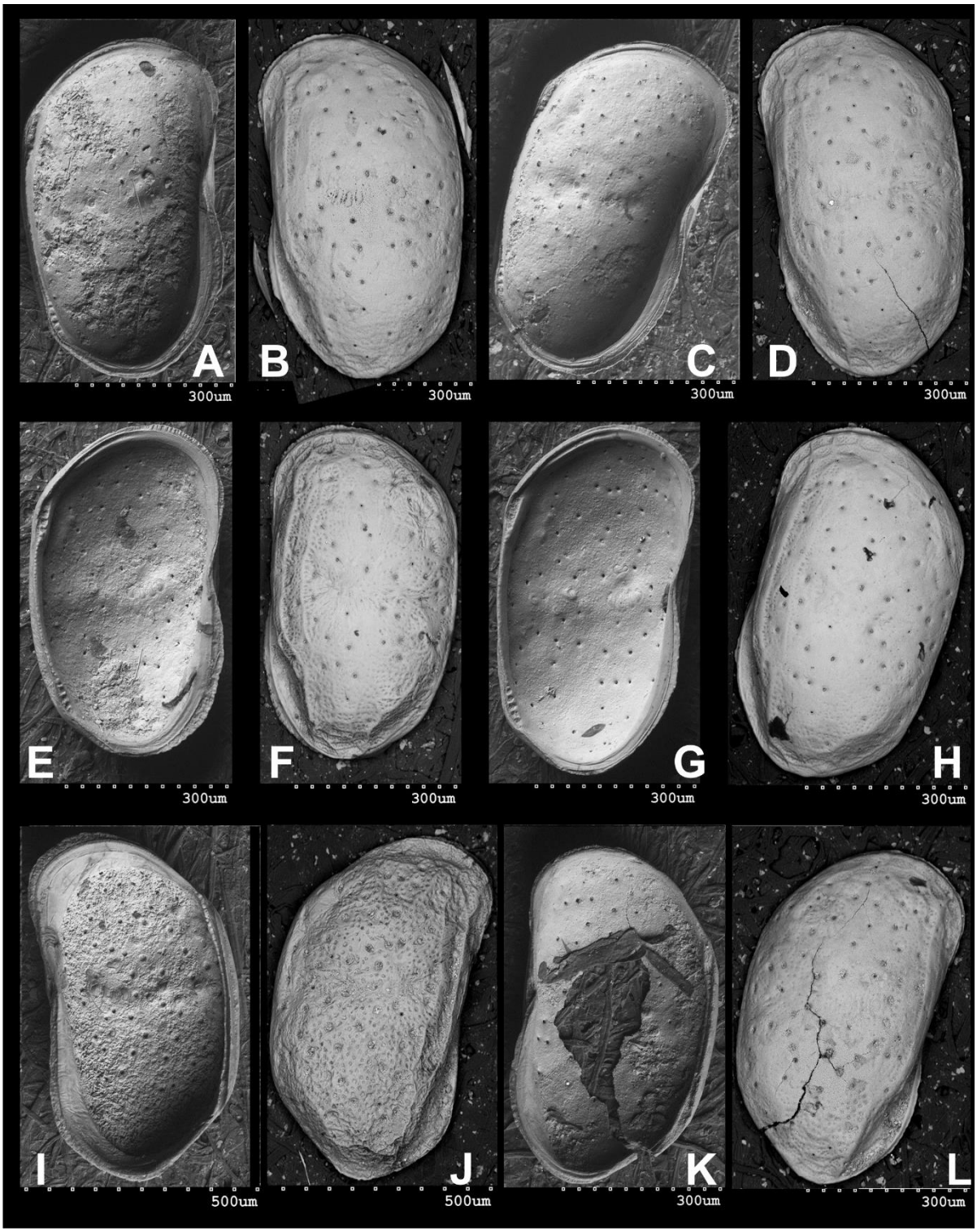

Fig. 3.12. All the ostracods are from the Sognsvann location. A-B: *Cythere lutea*, PMO 235.063/21. C-D: *Cythere lutea*, PMO 235.063/23. E-F: *Cythere lutea*, PMO 235.063/3. G-H: *Cythere lutea*, PMO 235.063/15. I-J: *Cythere lutea*, PMO 235.063/16. K-L: Unidentified ostracod species, PMO 235.063/19. All the identified species are oriented with anterior pointing up, the unidentified are not oriented.

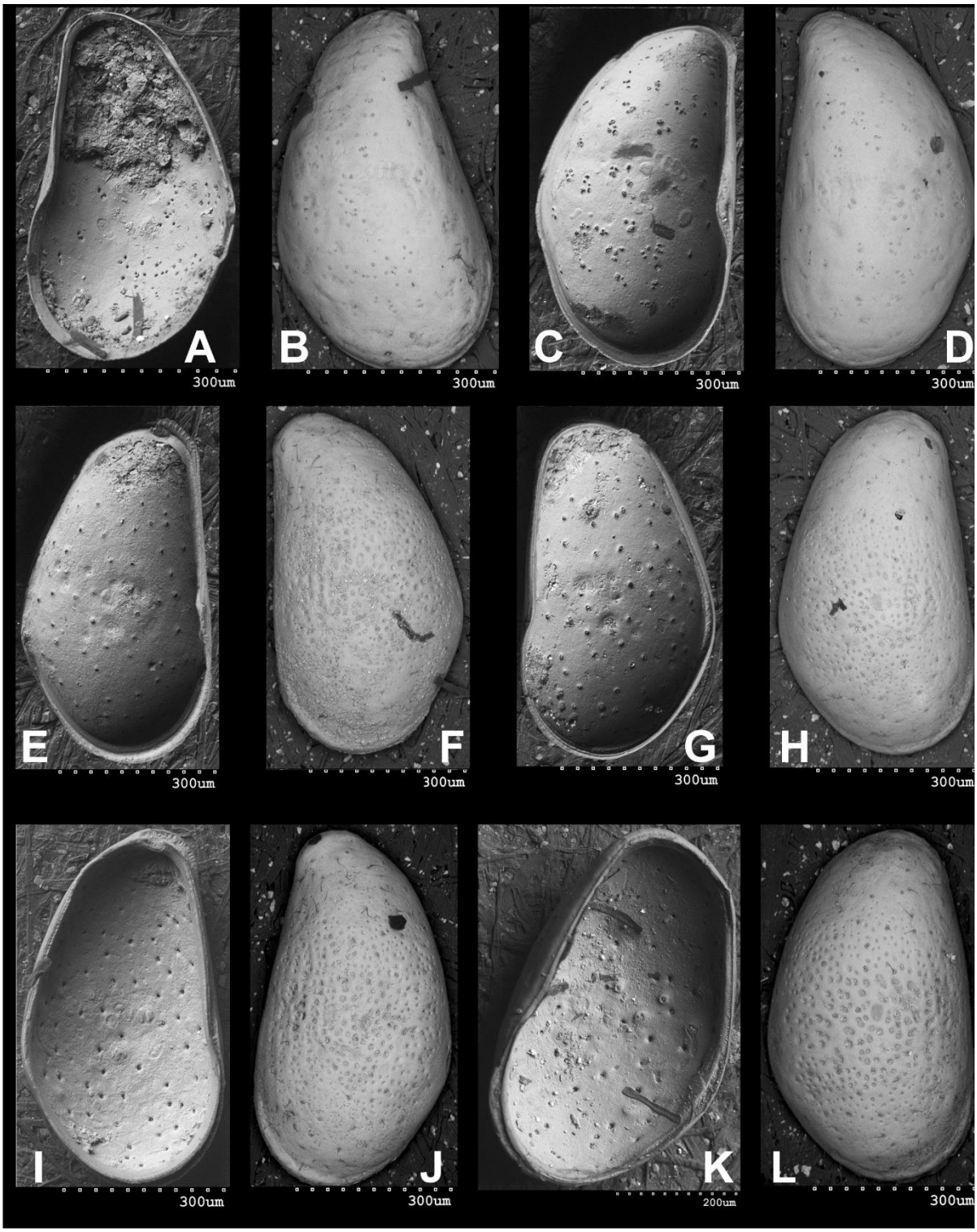

Fig. 3.13. All the ostracods are from the Sognsvann location. A-B: *Sarsicytheridea bradii*, PMO 235.063/4. C-D: *Sarsicytheridea bradii*, PMO 235.063/6. E-F: *Sarsicytheridea bradii*, PMO 235.063/7. G-H: *Sarsicytheridea bradii*, PMO 235.063/12. I-J: *Sarsicytheridea bradii*, PMO 235.063/24. K-L: Unidentified ostracod species, PMO 235.063/22. All the identified species are oriented with anterior pointing up, the unidentified are not oriented.

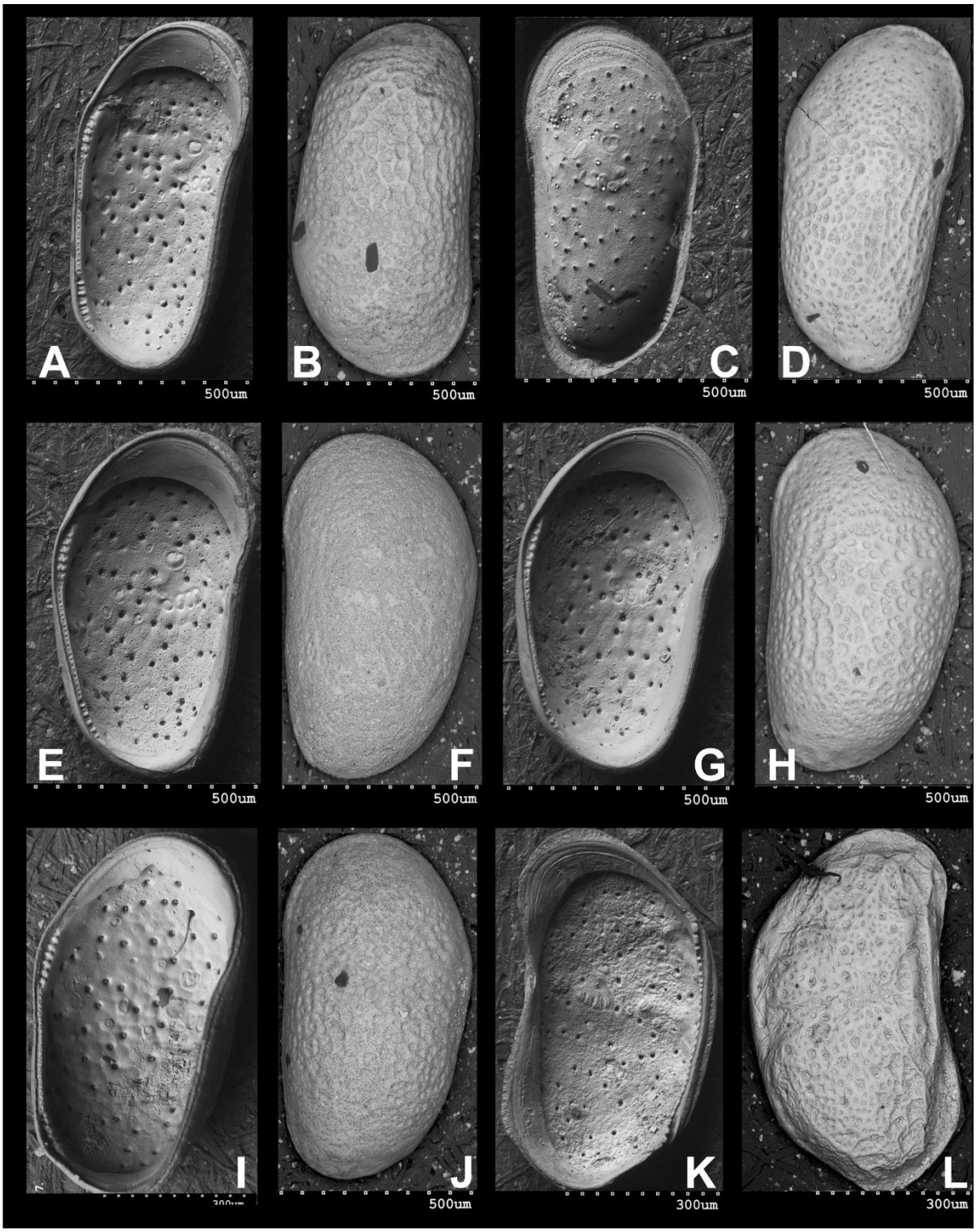

Fig. 3.14. All the ostracods are from the Sognsvann location. A-B: *Sarsicytheridea punctillata*, PMO 235.063/5. C-D: *Sarsicytheridea punctillata*, PMO 235.063/11. E-F: *Sarsicytheridea punctillata*, PMO 235.063/13. G-H: *Sarsicytheridea punctillata*, PMO 235.063/14. I-J: *Sarsicytheridea punctillata*, PMO 235.063/17. K-L: Unidentified ostracod species, PMO 235.063/20. All the identified species are oriented with anterior pointing up, the unidentified are not oriented.

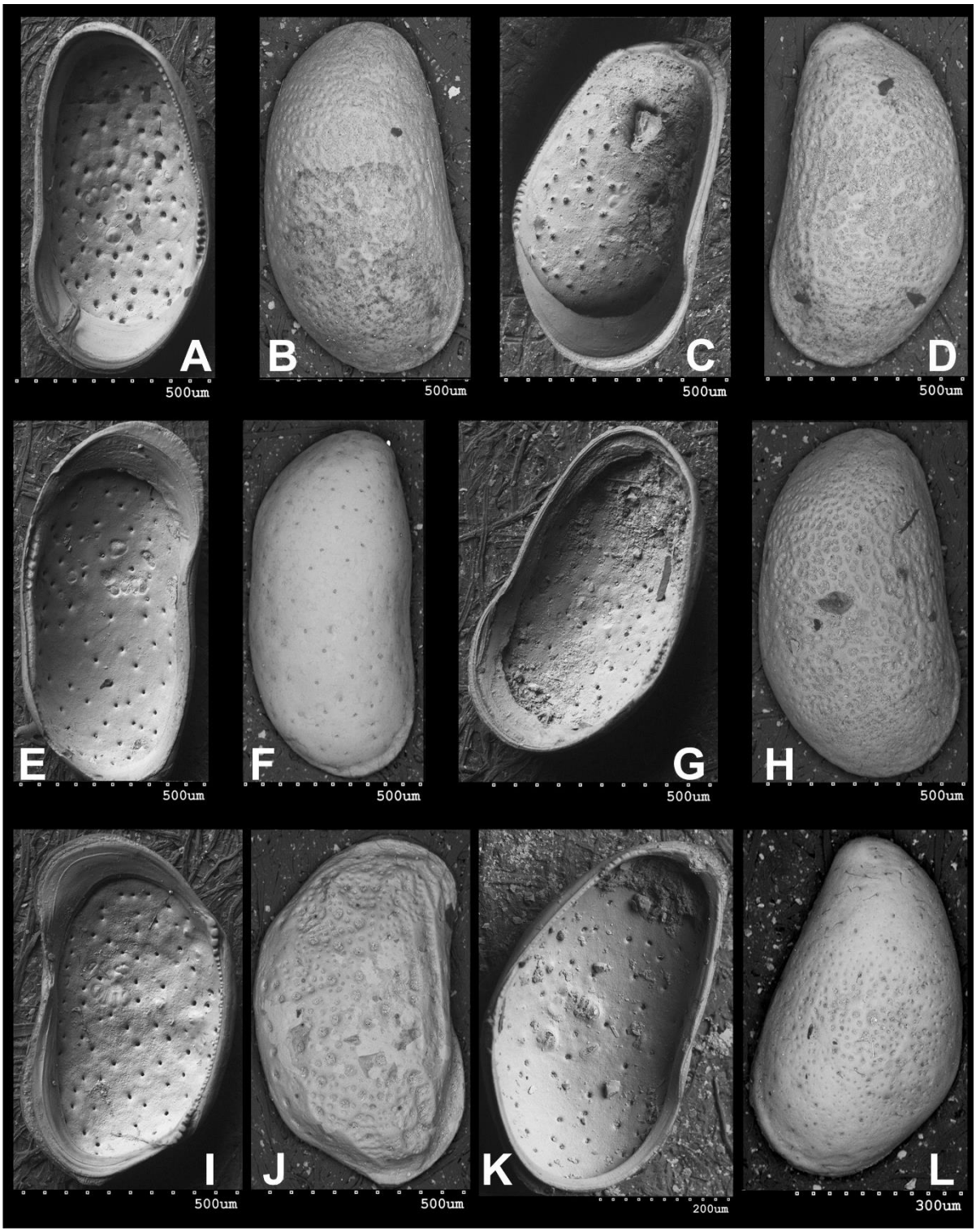

Fig. 3.15. All the ostracods are from the Sognsvann location. A-B: Unidentified ostracod species, PMO 235.063/1. C-D: Unidentified ostracod species, PMO 235.063/2. E-F: Unidentified ostracod species, PMO 235.063/8. G-H: Unidentified ostracod species, PMO 235.063/9. I-J: Unidentified ostracod species, PMO 235.063/10. K-L: Unidentified ostracod species, PMO 235.063/18. The pictures of these ostracods are not oriented in the same direction, anterior pointing up.

3.7 Species identification

The macrofauna at Sognsvann present in both boxes from the collection at the Natural History Museum was not fully determined because of the Covid-19 lockout but contains (Figs. 2.2 and 3.16):

Gastropods:

Euspira montagui, sandy and muddy sublittoral, 15 – 200m.

Roxania utriculus, muddy sand, sublittoral to 1500m.

Bivalves:

Mytilus edulis, upper shore to shallow sublittoral.

Mya truncata, mixed sandy, lower shore to 70m.

Hiatella arctica, lower shore to offshore.

Macoma calcarea, intertidal to offshore.

Balanus sp.

The habitat of all the species above were taken from WoRMS Editorial Board, (2020). Looking at the fauna from the Sognsvann location it seems to indicate shallow water (*Mytilus*), but the water depth was most likely deeper than 10m. *Mytilus edulis* is found to be an ideal nearshore palaeoceanographic proxy throughout much of the North Atlantic. Their environmental optimum is a salinity range of ~20 – 35 PSU (practical salinity units) and a temperature range of 10 – 20 °C (Wanamaker et al. 2007).

Fig. 3.16. The box of Sognsvann sample taken from the collection of the Natural History Museum, for species identification. The sample is from a level ca. 192m a.s.l. PMO 3520A.

4 Discussion

4.1 LA-ICPMS

The mollusc genus *Mytilus* is well suited to extract (paleo) environmental information thanks to its high longitudinal growth rate of its calcite shell layer, combined with large geographical distribution. It is also tolerant to a broad range of environmental conditions. Klein et al. (1996a) suggested that the Mg/Ca variations within the calcite shell layer of *Mytilus* can provide an accurate record of seasonal changes in sea surface temperatures. Dodd (1965) observed a seasonal variation, correlated with temperature, in the Mg content of *Mytilus edulis* shells. Although the variations can give a lot of information about the temperature, it is becoming clearer that mollusc shell chemistry is also affected by biological factors known as vital effects (Rosenberg & Hughes, 1991; Klein et al. 1996b). This implies that the environmental records could be obstructed by ontogenetic trends as well as by seasonal variations in the animal's physiology (Putten et al., 2000). Mg compares with temperature during spring, but this covariation is abruptly interrupted after the spring phytoplankton bloom (Putten et al., 2000). Though Mg and Sr cycles show great similarity with a maximum during spring and early summer, they cannot be explained only by seasonal variations in the seawater composition.

The observations of Putten et al. (2000) do not preclude that temperature may influence skeletal Mg incorporation, either directly or through a physiological factor that covaries with temperature. However, there was clearly no constant Mg/Ca temperature relationship within the same shell and temperature was clearly not the only controlling factor. They speculate there might be an (in)direct temperature control on skeletal Mg incorporation combined with a seasonal physiological effect, with the latter triggering their observed breakdown in the Mg/Ca temperature covariation.

Klein et al. (1996b) proposed a model that integrates salinity and metabolic rate to explain the variability of Sr/Ca and $^{13}C/^{12}C$ in shells of *Mytilus trossulus*. Although mollusc shells in general might be a good indicator of paleo-environmental reconstruction, a better understanding of the different factors controlling shell chemistry is required to correctly interpret the element profiles.

Sr/Ca and Mg/Ca ratios in the aragonite layer of *Mytilus edulis* shell increase linearly with increases in Sr/Ca and Mg/Ca solution ratios in the seawater. In the calcite layer of *Mytilus edulis* shell Sr/Ca ratios increase linearly with increases in Sr/Ca solution ratios, while Mg/Ca ratios increase exponentially with the Mg/Ca ratio in the culture solution (Lorens & Bender, 1980). Although the skeletal Sr/Ca variations in the study of Putten et al. (2000) varied by a factor of 1.3 to 1.8 over any given cycle, this was too large to be explained solely based on variations in the seawater Sr/Ca ratio. Dodd & Crisp (1982) showed that the Sr/Ca ratios of most estuarine waters only differ significantly from the open ocean ratios at salinities below 10‰. Klein et al. (1996b) suggested that the relationship between Sr/Ca ratios in seawater and the ratio in the calcite shell layer of *Mytilus trossulus* is complicated by the influence of mantle metabolic activity. They briefly suggested that the skeletal Sr/Ca ratio of individuals with a negligible mantle metabolic activity closely follows the seawater Sr/Ca ratio, whereas the skeletal Sr/Ca ratio in animals with a higher mantle metabolic activity is modified by the rate of Ca-pumping across the mantle. Although shell Sr/Ca and Mg/Ca ratios are not robust temperature proxies, Ba/Ca is proven to be a good proxy for salinity in *Ruditapes philippinarum* (Poulain et al., 2015) and for *Mytilus edulis* (Gillinkin et al., 2006).

$\delta^{18}O$ is shown to mostly be influenced by temperature and salinity (Epstein et al., 1953). This can be used for additional information on seasonality of the shell chemistry. Though Ba is proven to be a good indicator for salinity, combining these two proxies might make for a better understanding of paleoenvironment. Ba peaks may coincide with the annual algal biomass maximum and presumably reflect elevated concentrations of particulate Ba, associated with the spring phytoplankton bloom and diatom blossoms (Putten et al., 2000; Stecher et al., 1996). Elevated levels of Ba, both as suspended particulate and sedimentary barite, have been shown to be linked with oceanic regions of primary productivity (Goldberg & Arrhenius, 1958; Chow & Goldberg, 1960; Dehairs et al., 1980; Deharis et al., 1987; Bishop, 1988).

4.1.1 Skådalen

For the shell of *Mytilus edulis* from the Skådalen locality, which is ca. 4.5 cm in length. 81 points with ca. 500 µm distance were measured along the shell. Looking at the Ba values compared to distance from umbo (Fig. 3.2) the values shows tendencies for possible freshwater pulses at 0mm (umbo) to 4mm, this could possibly be the first living year of the specimen. Here it is interpreted as the first summer melting episode experienced by the shell (Fig. 3.2). The peak at 20mm is interpreted as age 1 years, at 26.5mm is interpreted as 2 years. There might be two more pulses, at 30.5mm (3 years) and 38mm (4 years). The number of peaks is in general agreement with the number of annual growth zones indicated by the CT images. Positive peaks in Ba values correspond to episodes of reduced salinity (Gillikin et al., 2006). These freshwater pulses could indicate the summer when temperatures rise and the glaciers release melt water. The freshwater results in brackish tendencies in the glacier front where the freshwater runs off into ocean. The peak at 20mm is very high compared to the other four. In addition to the decline in salinity, Ba peaks may coincide with the annual algal biomass maximum and presumably reflect elevated concentrations of particulate Ba (Putten et al., 2000). When comparing the *Mytilus edulis* Ba/Ca values from the Skådalen location (Fig. 3.3) to Gillikin et al. (2006: fig. 7), their values generally lie between 0 – 5 Ba/Ca (µmol/mol). They also have some peaks over 10 (µmol/mol), though the values in Fig. 3.3 are somewhat higher than theirs. Gillikin et al. (2006) found there was a good correlation between the Ba/Ca ratios in the lab grown *Mytilus edulis* and the Ba/Ca ratios of the water in which they grew.

Looking at the values of Mg and Sr for *Mytilus edulis* from the Skådalen locality they have similar trends. Fig. 3.2 shows small trends in declining Sr after the top of Ba, and when Ba increases to a new top, Sr follows, though these trends are not evident in both shells.

4.1.2 Sognsvann

The *Mytilus edulis* shell, ca. 7.8cm in length, from the Sognsvann locality. 156 points with ca. 500 µm distance were measured along the shell. There are nine peaks evident in the Ba curve, one at 2mm (umbo), 10mm (interpreted as age 1 year), 28mm (2 years), 36mm (3 years), 47.5mm (4 years), 62mm (5 years), 67mm (5 years), 69mm (6 years) (Fig. 3.5). As shown on Fig. 3.4 the analysis starts in the aragonite layer and transitions to the calcite layer towards the end of the shell. This might be the explanation for the wide top from ca. 45mm, to 62mm. There is a sharp transition from the highest peak at 55mm with a value of 68.13 ppm Ba, to 56.5mm with a value of 1.31 ppm Ba. There is also a sharp transition from 62mm with a value of 44.22 ppm Ba to 63.5mm with a value of 4.76 ppm Ba. This could indicate two periods of oscillation of the glacier. The rapid transitions can be partly explained by their locations toward the outer end of the shell where the growth rate has slowed (Wanamaker et al., 2007).

Looking at the curve in Fig. 3.6 of Ba/Ca (µmol/mol) *Mytilus edulis* from the Sognsvann location it is more difficult to compare to Gillikin et al. (2006; fig.7), their background values are around 0 – 5 (µmol/mol). Background values in Fig. 3.6 are primarily around 5 – 10 (µmol/mol) throughout the shell. There are also more peaks along the shell compared to Gillikin et al. (2006), which may indicate more fluctuation in the salinity of the seawater.

As indicated by Lorens & Bender (1980) the Mg/Ca and Sr/Ca ratios vary from the calcite layer to the aragonite layer. This may explain the relatively low values of Mg from umbo to 55.5mm (Fig. 3.5) followed by relatively higher values. Sr values seem to have the same wide top from 45mm to 62mm as the Ba curve. Mg has a relatively low concentration from umbo to 56mm, this would be an indication of the transition from the aragonite layer to the calcite layer. After 56mm the concentration increases, and the pulses are more visible. For the Skådalen shell there are cycles in Sr visible between the tops in Ba, the same cycles are not as visible in this shell.

There are no data on $\delta^{18}O$ for this shell and Ba can therefore not be compared to other data. However, the number of Ba peaks agrees with the number of growth zones in the CT images.

4.2 $\delta^{18}O$ and $\delta^{13}C$

The results of $\delta^{18}O$ analysis correspond well to the Ba results (Fig. 3.10). Negative values of $\delta^{18}O$ correspond to negative fluxes in salinity (MacLachlan et al., 2007; Wanamaker et al., 2007). The $\delta^{18}O$ values compared to approximate distance from umbo are shown in Fig. 3.10. Negative peaks in $\delta^{18}O$ values can represent warmer temperatures, but the negative values found here more likely reflect low salinity (MacLachlan et al., 2007). Three negative peaks are evident, around 3mm, 10mm and 17mm, broadly coinciding with Ba peaks and thus supporting freshwater input at these points. One could argue there is another negative peak at 30mm. This pointing to the shell experiencing four – five seasons of summer melting.

It is suggested that oxygen chemistry of biogenic carbonates ($\delta^{18}O_{calcite}$) is primarily controlled by water temperature and isotopic composition of water ($\delta^{18}O_{water}$; related to salinity) (Wanamaker et al., 2007). It has been shown that there are no noticeable trends in shell isotopic fractionation ($\delta^{18}O_{calcite}$ VPBD - $\delta^{18}O_{water}$ VSMOW) based on an animal's shell length, growth rate, or geographic origin (Wanamaker et al., 2007). *Mytilus edulis* bivalves are an accurate proxy for water temperature if $\delta^{18}O_{water}$ can be determined independently, and that *Mytilus edulis* deposit its shell ($\delta^{18}O_{calcite}$) in isotopic equilibrium with seawater (Wanamaker et al., 2007). Epstein et al. (1953) agreed in that $\delta^{18}O$ is only influenced by temperature and salinity and thus can provide information on the seasonality of shell chemistry. During a study of the salinity: $\delta^{18}O$ water relationship in Kongsfjorden, western Spitsbergen, MacLachlan et al. (2007) found the main source of freshwater in the fjord was from ice melting during spring and summer, not the seasonal precipitation or sea ice melting. Assuming the conditions in the Oslo area during the earliest Holocene were similar to the conditions in Spitsbergen, the main source of freshwater recorded in the shell of *Mytilus edulis* used in this study could be of ice melting origin. They also found low values in $\delta^{18}O$ correspond to low salinity while high values in $\delta^{18}O$ correspond to high salinity.

Skeletal $\delta^{13}C$ shows seasonal variations, characterized by a minimum that coincides with a Mn maximum (Putten et al., 2000). $\delta^{13}C$ variations are not in equilibrium with the seasonal $\delta^{13}C$ trend of the seawater DIC and presumably reflect fluctuations in the contribution of metabolic carbon to the shell carbonate, corresponding to seasonal variations in the mussel's respiration rate. In this study Mn was not measured and can therefore not be compared to $\delta^{13}C$. The strong vital effects on carbon isotopes in *Mytilus edulis* make environmental interpretation difficult (Putten et al., 2000; Klein et al., 1996b).

4.3 Ostracods

After SEM imaging 24 ostracods, three species were identified (Fig. 3.12 – 3.15). *Cythere lutea* and *Sarsicytheridea bradii* both tolerate salinities >5 - >30‰, being meso-, poly- and euhaline taxa. They live in shallow water to deep, open sea. The presence of these species is consistent with the Sognsvann location being near the glacier front at the time of deposition. Though the sieved sample from Sognsvann were of finer material indicating this locality being from deeper water. In contrast to the other field samples MG1, MG2, MG4 and partially MG3, being poorly sorted glacial material, washed in the surf zone, indicating shallower water than for the Sognsvann locality.

Sarsicytheridea punctillata is a species which tolerates a wide range of salinities (3.8 >30‰), from oligohaline to mesohaline, polyhaline and euhaline conditions. They live from very shallow to shallow water (Stepanova et al., 2019). Ingram (1998) studied the palaeoecology and geochemistry of shallow marine ostracods from the Sand Hole formation, inner Silver Pit, southern North Sea. She found the environmental factors that most affect ostracods physiologically are salinity, temperature and ionic composition of the water. There is no uptake of calcium once the shell has been fully calcified. Ingram therefore did extensive studies of the elemental composition of ostracod shells and found the genus *Sarsicytheridea* a promising source of trace element analyses, yielding a positive correlation between Mg/Ca and temperature. Ostracod moult processes are short, so a single ostracod valve represents the environmental conditions of the ambient water mass at the time of calcification (usually a few hours). Using a specific species allows close constraints to be placed on the timing and environmental setting of shell construction. There was not time to do trace element analyses on the ostracods.

4.4 Radiocarbon dating

Historical localities near Grefsenkollen (Fig. 1.2) have been studied by Brøgger (1901) and Holtedahl (1960). Some new radiocarbon datings of historic localities are introduced, showing the marine limit at ca. 220 m a.s.l. may have been older than previously thought. Vardeåsen, Nesodden, at 176 m a.s.l (Fig. 1.2) is not a classic marine limit locality, though the fauna is very interesting with similar species as the marine limit in the Oslo area. The fauna indicates deeper water than the shoreline, though the water depth from which the material is from is not known. At a historical locality from the Aker substage at Grefsenkollen, Gjessing & Spjeldnaes (1979) found and radiocarbon dated *Balanus balanus* and discussed their findings in relation to the Skådalen locality. They found the difference in age corresponded to a 30m difference in sea level between the two localities. According to their dating of *Balanus balanus* the sealevel at Grefsen were 250m a.s.l., which does not correspond to Skådalen being the marine limit at 221m a.s.l.

The timeline (Fig. 4.1) shows an attempt to illustrate the placement of the PBO relative to the Ås-Ski substage and the Aker substage. New datings done in this thesis are placed relative to each substage. The end of Younger Dryas epoch has been radiocarbon dated through ice cores to 11,653 ± 99 cal yr BP. (Rasmussen et al., 2007). Andersen et al. (1995) dated the Ski moraine to 10,170 ± 190 C^{14} years, this age had however been reservoir corrected with 440 years. Adding 440 years to the age before calibrating, the age of the Ski moraine ends up being 11,895 cal yr BP, which may indicate both the Ra substage and the Ås-Ski substage are older than the end of Younger Dryas.

The Skådalen dating is assumed to date the marine limit at 220m a.s.l. *Mytilus edulis* was radiocarbon dated and gave a median age of 11,262 cal yr BP. *Balanus* sp. from the same locality was radiocarbon dated with a median age of 6717 cal yr BP, which does not correspond with the *Mytilus edulis* datings. This problem was encountered by Holtedahl (1960) when discussing radiocarbon dating of *Mytilus edulis* and *Balanus* sp. from Skådalen. He reported ages of *Mytilus edulis*, 9450 ± 250 and 9250 ± 250 ^{14}C years and *Balanus* sp., 7300 ± 190 ^{14}C years. The reason for this inconsistency is not known, though the material of *Balanus* sp. might have been misplaced at some point. The Sognsvann dating at 192m a.s.l. has a median age of 11,150 cal yr BP and the Nesodden dating has a median age of 10,877 cal

yr BP. The Skådalen and Sognsvann localities were probably both situated slightly outside the main ridge of the Aker moraine.

There is some debate to the age of the Aker substage, though the Grefsen moraine was dated to 10,499 cal yr BP. (Gjessing & Spjaldnaes, 1979). During construction work at Skådalen, Henningsmoen & Spjeldnæs (1991) found fragments of *Mytilus* and *Macoma* shells south of Skådalen station at 205m a.s.l. They dated the shells to 10,505 ± 145 C^{14} years which gives a median age of 11,699 cal yr BP, close in age to the end of Younger Dryas and slightly older than the Skådalen dating done in this thesis. This is interesting seeing the sediments and organic inner linings of foraminifera found with the shells indicated Preboreal age or older. They also found a good profile 325m south of Skådalen station at 185m a.s.l., after a pollen analysis they determined the material found there was of Preboreal age. After dating a *Mytilus* shell from this location they found an age of 9610 ± 90 C^{14} years, calibrated median age is 10,484 cal yr BP suggesting the material from the marine limit 221m a.s.l. in (Holtedahl, 1960; Nydal, 1960) might have been incorrectly labeled and in reality have been from this location at 185m a.s.l.

This thesis has attempted to locate the PBO in relation to the substages. In this timeline there are two possible ages of the PBO presented. 11,400 – 11,500 cal yr BP (Rasmussen et al., 2007) which places the PBO toward the Ås-Ski substage or 10,800 cal yr BP (Hald & Hagen, 1998) which places the PBO toward the Aker substage, which seems more likely. The youngest age also corresponds well to the dating of an interval of very high sedimentation rate in a core analyzed by Hammer & Webb (2010) from Snarøya.

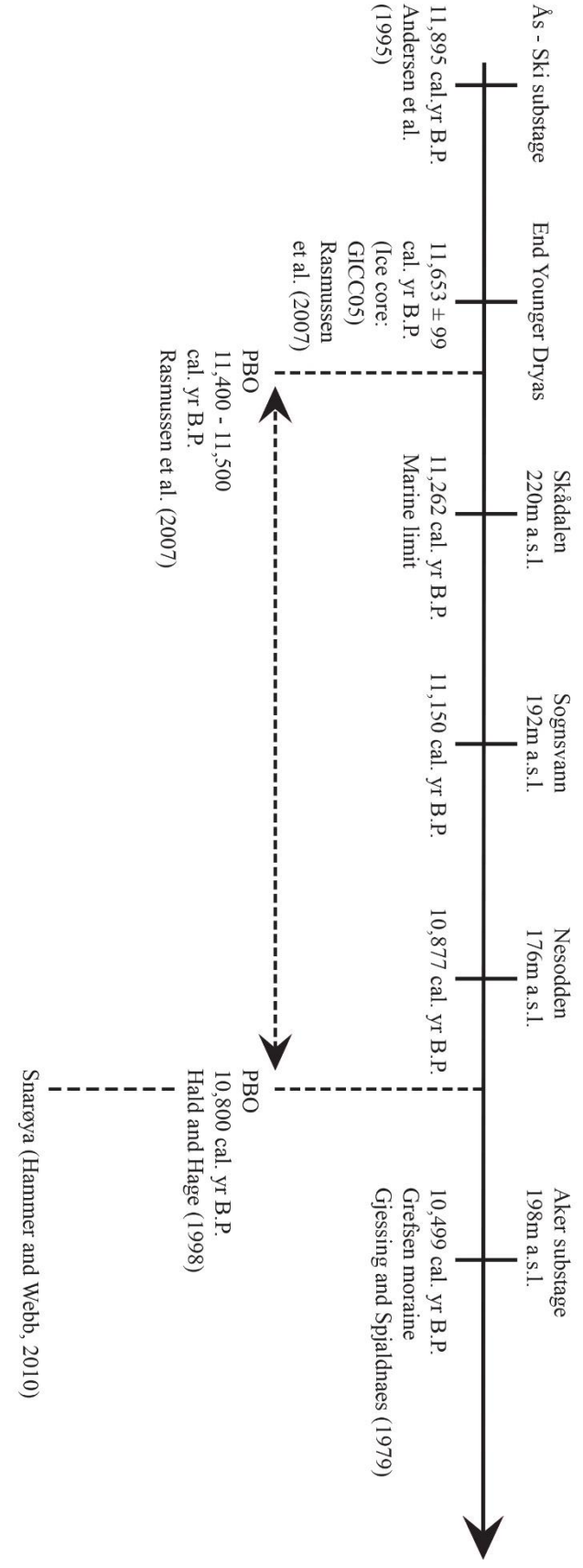

Fig. 4.1. A timeline from the end Younger Dryas to the Aker substage. All ages mentioned are calibrated years B.P.

5 Conclusion

- The evidence presented (Ba, $\delta^{18}O$ profiles and ostracod fauna) indicate or is consistent with freshwater input at the Skådalen and Sognsvann localities, interpreted as deposition in relation to the front of the ice-cap.

- The timeline presented attempts to place the PBO in relation to the substages. The PBO can be linked either with the Ås – Ski substage with an age of 11,400 – 11,500 cal yr BP, or more likely with the Aker substage with an age of 10,800 cal yr BP correlating well with the datings from the core at Snarøya (Hammer & Webb, 2010). It also suggests the Ra substage and Ås-Ski substage may be older than the end of Younger Dryas. The new datings correspond well with the Aker substage, but indicated the localities sampled are located outside the moraine ridge of the Aker substage.

Further study:

- Trace metal analysis of the ostracods, for correlation with the trace metal analysis of *Mytilus edulis* from the Sognsvann locality.

- Investigate and correlate the substages in Norway with the moraines in Sweden and other nearby countries.

- Using a drill in the existing holes from the LA-ICPMS analysis performed on the *Mytilus edulis* shells giving a higher resolution of the $\delta^{18}O$ curve and a better foundation for comparison with the Ba curve.

- Including Mn in the LA-ICPMS analysis for correlation with $\delta^{13}C$.

References

Allaby, M. (2009). *A Dictionary of Zoology.* 3 ed. Oxford: Oxford University Press. Available from: https://www-oxfordreference-com.ezproxy.uio.no/view/10.1093/acref/9780199233410.001.0001/acref-9780199233410-e-6205?rskey=Pg3Zd6&result=1 (Accessed: June 14, 2020)

Allaby, M. (2020). «de Geer moraine». *A Dictionary of Ecology.* Available from: Encyclopedia.com: https://www.encyclopedia.com/science/dictionaries-thesauruses-pictures-and-press-releases/de-geer-moraine-0 (Accessed: May 23, 2020)

Andersen, B. G., Mangerud, J., Sørensen, R., Reite, A., Sveian, H., Thoresen, M., Bergstrøm, B. (1995). Younger dryas ice-marginal deposits in Norway. *Quaternary International*, (28), 147 – 169. https://doi.org/10.1016/1040-6182(95)00037-J

Behre, K. E. (1978). Die Klimaschwankungen im europäischen Präboreal. Herrn Prof. Dr. sc. Heinz Kliewe zum 60. Geburtstag gewidmet. (Les variations climatiques en Europe au cours du Préboréal. En 52omage au Prof. Kliewe pour son 60 anniversaire). *Petermanns Geographische Mitteilungen Gotha*, 122(2), 97-102.

Bishop, J. K. B. (1988). The barite-opal-organic carbon association in oceanic particulate matter. *Nature* 332**,** 341–343 (1988). https://doi-org.ezproxy.uio.no/10.1038/332341a0

Björck, S., Kormer, B., Johnsen, S., Bennike, O., Hammarlund, D., Lemdahl, G., Possnert, G., Rasmussen, T. L., Wohlfarth, B., Hammer, C. U., Spurk, M. (1996). Synchronized terrestrial-atmospheric deglacial records around the North Atlantic. *Science*, 274, 1155 – 1160.

Björck, S., Rundgren, M., Ingolfsson, O., Funder, S. (1997). The preboreal oscillation around the Nordic Seas: terrestrial and lacustrine responses. *Journal of Quartinary Science: Published for the Quartinary Reserch Association*, 12(6), 455 – 465. https://doi.org/10.1002/(SICI)1099-1417(199711/12)12:6<455::AID-JQS316>3.0.CO;2-S

Bjørklund, K. R., Kruglikova, S. B., Hammer, Ø. (2019). The radiolarian fauna during the Younger Dryas–Holocene transition in Andfjorden, northern Norway. *Polar Research, 38*. https://doi.org/10.33265/polar.v38.3444

Brøgger, W. C. (1901). Om de senglaciale og postglaciale nivåforandringer i Kristianiafeltet (Molluskfaunan). *Norges Geologiske Undersøkelse*, 31, 731 pp + 19 plates.

Chow, T. J., Goldberg, E. D. (1960). On the marine geochemistry of barium. *Geochimica et Cosmochimica Acta*, 20(3-4), 192 – 198. https://doi.org/10.1016/0016-7037(60)90073-9

Davis, B. A. S., Brewer, S., Stevenson, A. C., Guiot, J., (2003). The temperature of Europe during the Holocene reconstructed from pollen data. *Quaternary Science Reviews* 22, 1701 – 1716. https://doi.org/10.1016/S0277-3791(03)00173-2

Dehairs, F., Chesselet, R., Jedwab, J. (1980). Discrete suspended particles of barite and the barium cycle in the open ocean. *Earth and Planetary Science Letters*, 49(2), 528 – 550. https://doi.org/10.1016/0012-821X(80)90094-1

Deharis, F., Lambert, C. E., Chesselet, R., Risler, N. (1987). The biological production of marine suspended barite and the barium cycle in the Western Medeterranean Sea. *Biogeochemistry*, 4(2), 119 – 140. https://doi.org/10.1007/BF02180151

Dodd, J. R. (1965). Environmental control of strontium and magnesium in *Mytilus*. *Geochimica et Cosmochimica Acta*, 29(5), 385 – 398. https://doi.org/10.1016/0016-7037(65)90035-9

Dodd, J. R., Crisp, E. L. (1982). Non-linear variations with salinity of Sr/Ca and Mg/Ca ratios in water and aragonitic bivalve shells and implications for paleosalinity studies. *Palaeogeography, Palaeoclimatology, Palaeoecology*, 38(1-2), 45 – 56. https://doi.org/10.1016/0031-0182(82)90063-3

Epstein, S., Buchsbaum, R., Lowenstam, H. A., Curey, H. (1953). Revised carbonate-water isotopic temperature scale. *Geological Society of America Bulletin*, 64(11), 1315 – 1326. https://doi.org/10.1130/0016-7606(1953)64[1315:RCITS]2.0.CO;2

Feyling-Hanssen, R. (1964). Foraminifera in Late Quatenary deposits from the Oslofjord area. *Norges Geologiske* Undersøkelse, 225, 383 pp.

Gillikin, D. P., Dehairs, F., Lorrain, A., Steenmans, D., Baeyens, W., André, L. (2006). Barium uptake into shells of the common mussel (Mytilus edulis) and the potential for estuarine paleo-chemistry reconstruction. *Geochimica et Cosmochimica Acta*, 70(2), 395 – 407. https://doi.org/10.1016/j.gca.2005.09.015

Gjessing, J., Spjeldnaes, N. (1979). Datings of the Grefsen moraine and remarks on the deglaciation of southern Norway. *Norwegian journal of geography*, 33, 71 – 81. https://doi.org/10.1080/00291957908621925

Goldberg, E. D., Arrhenius, G. O. S. (1958). Chemistry of Pacific pelagic sediments. *Geochimica et Cosmochimica Acta*, 13(2-3), 199 – 212. https://doi.org/10.1016/0016-7037(58)90046-2

Hald, M., Hagen, S. (1998). Early Preboreal cooling in the Nordic seas region triggered by meltwater. *Geology*, 26(7), 615 – 618. https://doi.org/10.1130/0091-7613(1998)026<0615:EPCITN>2.3.CO;2

Hammer, Ø., Webb, K. E. (2010). Piston coring of Inner Oslofjord pockmarks, Norway. *Norwegian Journal of Geology*, 90, 79 – 91.

Henningsmoen, K. E., Spjeldnæs, N. (1991) Kvartærdateringer fra Skådalen ved Oslo. *Abstract in Geonytt*, 18, 26.

Holtedahl, O. (1960). Geology of Norway. *Norges Geologiske Undersøkelse*, 208, 552 pp.

Ingram, C. (1998). Palaeoecology and geochemistry of shallow marine ostracoda from the Sand Hole formation, Inner Silver Pit, southern North Sea. *Quaternary Science Reviews*, 17(9-10), 913 – 929. https://doi.org/10.1016/S0277-3791(98)00025-0

Jochum, K. P., Weis, U., Stoll, B., Kuzmin, D., Yang, Q., Raczek, I., Jacob, D. E., Stracke, A., Birbaum, K., Frick, D, A., Günther, D., Enzweiler, J. (2011). Determination of Reference Values for NIST SRM 610-617 Glasses Following ISO Guidelines. *Geostandards and geoanalytical research*, 35(4), 397 – 429. https://doi.org/10.1111/j.1751-908X.2011.00120.x

Kautsky, N. (1982). Growth and size structure in a Baltic *Mytilus edulis* population. *Marine Biology*, 68(2), 117 – 133. https://doi-org.ezproxy.uio.no/10.1007/BF00397599

Klein, R. T., Lohmann, K. C., Thayer, C. W. (1996a). Bivalve skeletons record seas-surface temperature and $\delta^{18}O$ via Mg/Ca and $^{18}O/^{16}O$ ratios. *Geology*, 24(5), 415 – 418. https://doi.org/10.1130/0091-7613(1996)024<0415:BSRSST>2.3.CO;2

Klein, R. T., Lohmann, K. C., Thayer, C. W. (1996b). Sr/Ca and $^{13}C/^{12}C$ ratios in skeletal calcite of Mytilus trossulus: Covariation with metabolic rate, salinity, and carbon isotopic

composition of seawater. *Geochimica et Cosmochimica Acta*, 69(21), 4207 – 4221. https://doi.org/10.1016/S0016-7037(96)00232-3

WoRMS Editorial Board (2020). World Register of Marine Species. Available from: http://www.marinespecies.org at VLIZ. (Accessed 2020-05-09). doi:10.14284/170

Lorens, R. B., Bender, M. L. (1980). The impact of solution chemistry on *Mytulis edulis* calcite and aragonite. *Geochimica et Cosmochimica Acta*, 44(9), 1265 – 1278. https://doi.org/10.1016/0016-7037(80)90087-3

Lønne, I., Nemec, W., Blikra, L. H., Lauritsen, T. (2001). Sedimentary architecture and dynamic stratigraphy of a marine ice-contact system. *Journal of Sedimentary Research*, 71(6), 922 – 943. Doi:https://doi-org.ezproxy.uio.no/10.1306/030901710922

MacLachlan, S. E., Cottier, F. R., Austin, W. E., Howe, J. A. (2007). The salinity: $\delta^{18}O$ water relationship in Kongsfjorden, western Spitsbergen. *Polar Research*, 26(2), 160 – 167. https://doi.org/10.1111/j.1751-8369.2007.00016.x

Nydal, R. (1960) Trondheim natural radiocarbon measurements II. *Radiocarbon*, 2, 82 – 96. https://doi.org/10.1017/S1061592X00020627

Poulain, C., Gillikin, D. P., Thébault, J. M., Bohn, M., Rogert, R., Paulet, Y.-M., Lorrain, A. (2015). An evaluation of Mg/Ca, Sr/Ca, and Ba/Ca ratios as environmental proxies in aragonite bivalve shells. *Chemical geology*, 396, 42 – 50. https://doi.org/10.1016/j.chemgeo.2014.12.019

Putten, E. V., Dehairs, F., Keppens, E., Baeyens, W. (2000). High resolution distribution of trace elements in the calcite shell layer of modern Mytilus edulis: Environmental and biological controls. *Geochimica et Cosmochimica Acta*, 64(6), 997 – 1011. https://doi.org/10.1016/S0016-7037(99)00380-4

Rasmussen, S. O., Vinther, B. M., Clausen, H. B., Andersen, K. K. (2007). Early Holocene climate oscillations recorded in the Greenland ice cores. *Quaternary Science Reviews* 26, 1907 – 1914. https://doi.org/10.1016/j.quascirev.2007.06.015

Reimer, L. (2013). *Scanning electron microscopy; physics of image formation and microanalyses*. Second edition. New York: Springer.

Rosenberg, G. D., Hughes, W. W. (1991). A metabolic model for the determination of shell composition in the bivalve mollusc, Mytilus edulis. *Lethaia*, 24(1), 83 – 96. https://doi.org/10.1111/j.1502-3931.1991.tb01182.x

Seed, R. (1976) Ecology, in Bayne, B. L. and Bayne, B. L. (eds.) *Marine mussels: their ecology and physiology* (vol. 10). Cambridge: Cambridge University Press, 13 - 65.

Stepanova, A., Obrochta, S., Quintana Krupinski, N. B., Hyttinen, O., Kotilainen, A., & Andrén, T. (2019). Late Weichselian to Holocene history of the Baltic Sea as reflected in ostracod assemblages. *Boreas*, 48(3), 761 – 778. https://doi.org/10.1111/bor.12375

Stuiver, M., Reimer, P.J., and Reimer, R.W. (2020), CALIB 7.1, WWW program at http://calib.org

Sørensen, R. (1979). Late Weichselian deglaciation in the Oslofjord area, south Norway. *Boreas*, 8(2), 241-246. https://doi.org/10.1111/j.1502-3885.1979.tb00806.x

Wanamaker Jr, A. D., Kreutz, K. J., Borns Jr, H. W., Introne, D. S., Feindel, S., Funder, S., Rawson, P. & Barber, B. J. (2007). Experimental Determination of Salinity, Temperature, Growth, and Metabolic Effects on Shell Isotope Chemistry of Mytilus edulis Collected from Maine and Greenland. *Paleoceanography*, 22(2). https://doi.org/10.1029/2006PA001352

Appendix 1: Table of LA-ICPMS results for Skådalen

Results of LA-ICPMS analyses of *M. edulis* from the Skådalen locality.

Results for LA-ICPMS of *M. edulis* shell from the Skådalen locality								
	Mg (ppm)	1sigma	Ca (ppm)	1sigma	Sr (ppm)	1sigma	Ba (ppm)	1sigma
610-01	401.31	52.53	81476	2577.09	465.38	139.31	416.49	61.5
610-02	399.71	52.24	81476	2577.09	465.27	138.43	417.19	61.34
610-03	412.12	53.8	81476	2577.13	483.42	142.99	433.32	63.48
Skjell-01	1116.9	145.72	400000.25	12650.12	1337.49	393.38	17.3	2.53
Skjell-02	821.1	107.12	400000.25	12650.49	1322.22	386.8	16.55	2.41
Skjell-03	635.98	83	400000.25	12650.44	1159.27	337.38	12.68	1.84
Skjell-04	522.31	68.22	400000.25	12650.46	1116.97	323.48	14.09	2.05
Skjell-05	530.5	69.38	400000.25	12650.56	1114.07	321.13	9.7	1.41
Skjell-06	418.99	54.89	400000.28	12650.48	1482.86	425.53	26.39	3.83
Skjell-07	450.69	59.18	400000.28	12650.45	1389.07	396.94	25.26	3.66
Skjell-08	711.88	93.72	400000.28	12650.45	1247.3	355	19.53	2.83
Skjell-09	632.09	83.47	400000.28	12650.45	1352.33	383.45	23.44	3.41
Skjell-10	601.26	79.67	400000.28	12650.5	1189.29	336.02	20.43	2.97
Skjell-11	561.16	74.65	400000.28	12650.54	1255.68	353.6	16.25	2.37
Skjell-12	1175.22	156.99	400000.28	12650.68	1517.75	426.07	20.79	3.04
Skjell-13	705.8	94.72	400000.28	12650.65	1316.71	368.56	15.5	2.27
Skjell-14	883.15	119.11	400000.28	12650.82	1178.51	328.99	13.27	1.95
Skjell-15	558.64	75.75	400000.28	12650.83	1313.88	365.87	10.53	1.55
610-04	132.25	18.03	81475.91	2576.81	256.88	71.37	3.1	0.46
610-06	479.39	65.76	81476.01	2577.21	604.9	167.71	524.4	78.03
610-05	494.79	68.29	81476.01	2577.2	612.02	169.36	528.89	79.07
Skjell-16	887.13	123.24	400000.28	12650.3	1355.06	374.34	14.6	2.19
Skjell-17	810.86	113.41	400000.28	12650.2	1310.49	361.48	11.14	1.68
Skjell-18	812.54	114.44	400000.31	12650.22	1327.21	365.61	12.82	1.95
Skjell-19	1034.56	146.77	400000.31	12650.34	1429.82	393.41	12.99	1.99
Skjell-20	768.15	109.79	400000.31	12650.21	1288.21	354.1	7.45	1.14
Skjell-21	701.41	101.82	400000.31	12650.46	1369.76	375.96	20.84	3.24
Skjell-22	541.31	79.21	400000.28	12650.33	1184.53	324.96	12.69	1.99
Skjell-23	452.92	66.82	400000.31	12650.4	1127.52	309.21	6.52	1.03
Skjell-24	514.09	76.47	400000.28	12650.28	1150.75	315.52	6.58	1.05
Skjell-25	396.84	59.53	400000.31	12650.27	1255.87	344.33	7.51	1.2
Skjell-26	585.58	88.6	400000.31	12650.32	1440.99	395.13	9.65	1.55
Skjell-27	606.31	92.54	400000.31	12650.34	1471.83	403.67	14.92	2.42
Skjell-28	597.99	92.07	400000.31	12650.48	1456.43	399.6	26.62	4.35
Skjell-29	780.42	121.23	400000.31	12650.53	1559.28	428.02	60.88	10.02
Skjell-30	765.09	119.91	400000.31	12650.32	1449.31	398.08	45.12	7.48
610-09	448.12	70.87	81476.01	2577.12	559.61	153.82	484.87	81.02
610-08	457.93	73.08	81476.02	2577.13	563.64	155.06	487.48	82.08

610-07	479.18	77.17	81476.02	2577.14	575.41	158.45	493.91	83.8
Skjell-31	540.64	87.87	400000.34	12650.36	1135.64	313.05	26	4.45
Skjell-32	371.84	60.99	400000.34	12650.3	1104.51	304.82	14	2.41
Skjell-33	314.36	52.04	400000.34	12650.26	1221.63	337.57	25.8	4.48
Skjell-34	405	67.67	400000.34	12650.24	1089	301.33	7.53	1.32
Skjell-35	430.01	72.52	400000.34	12650.31	1076.14	298.21	6.96	1.23
Skjell-36	385.43	65.6	400000.31	12650.2	1210.35	335.91	5.9	1.05
Skjell-37	461.97	79.36	400000.31	12650.2	1190.13	330.83	7.77	1.39
Skjell-38	448.76	77.81	400000.34	12650.27	1110.23	309.15	8.31	1.5
Skjell-39	583.23	102.07	400000.31	12650.21	1122.3	313.07	18.02	3.28
Skjell-40	777.99	137.42	400000.34	12650.24	1054.35	294.65	33.13	6.08
Skjell-41	552.35	98.47	400000.31	12650.26	1179.86	330.36	171.18	31.64
Skjell-42	617.48	111.1	400000.34	12650.3	1150.22	322.7	161.29	30.04
Skjell-43	623.16	113.16	400000.34	12650.37	1098.94	308.95	33.51	6.29
Skjell-44	550.14	100.82	400000.31	12650.49	1127.25	317.57	8.64	1.64
Skjell-45	618.23	114.34	400000.34	12650.5	1189.34	335.79	5.35	1.02
610-10	444.19	82.9	81476.02	2577.14	525.16	148.6	457.27	87.82
610-11	428.18	80.64	81476.02	2577.12	508.47	144.2	446.06	86.32
610-12	420.4	79.89	81476.02	2577.12	501.7	142.61	442.08	86.2
Skjell-46	501.84	96.23	400000.34	12650.47	1022.57	291.36	5.75	1.13
Skjell-47	504.4	97.59	400000.31	12650.35	1023.52	292.34	4.16	0.82
Skjell-48	400.64	78.21	400000.34	12650.31	983.38	281.56	6.36	1.27
Skjell-49	387.04	76.23	400000.38	12650.29	1065.1	305.72	5.23	1.05
Skjell-50	589.73	117.18	400000.34	12650.27	1034.04	297.55	5.12	1.04
Skjell-51	587.99	117.86	400000.34	12650.16	922.6	266.16	5.35	1.09
Skjell-52	333.69	67.47	285880.44	9041.06	780.99	225.89	4.35	0.89
610-13	422.41	86.15	81476.02	2577.14	491.75	142.61	434.2	89.77
610-14	410.42	84.43	81476.02	2577.13	481.49	140	426.17	88.74
610-15	401.65	83.33	81476.02	2577.13	473.54	138.06	421.16	88.31
610-16	436.45	23.73	81475.99	2577.21	521.99	101	457.64	18.15
610-17	429.12	23.35	81475.98	2577.21	517	100.05	451.57	17.92
610-18	426.74	23.27	81475.99	2577.15	509.07	98.54	445.75	17.71
Skjell-53	501.45	27.43	400000.19	12650.43	1117.89	216.45	6.28	0.25
Skjell-54	593.81	32.63	400000.19	12650.45	1147.59	222.27	6.95	0.28
Skjell-55	631.31	34.87	400000.22	12650.07	1068.64	207.05	5.84	0.24
Skjell-56	521.78	29.01	400000.19	12650.17	1116.44	216.39	6.74	0.27
Skjell-57	569.47	31.9	400000.19	12650.14	1027.57	199.24	9.29	0.38
Skjell-58	492.82	27.85	400000.19	12650.11	1059.7	205.56	11.06	0.45
Skjell-59	442.49	25.24	400000.22	12650.27	1210.89	234.99	21.34	0.87
Skjell-60	451.14	26	400000.22	12650.22	1153.88	224.04	18.96	0.78
Skjell-61	558.59	32.56	400000.19	12650.22	1095.49	212.81	14.66	0.61
Skjell-62	500.14	29.5	400000.19	12650.27	1125.79	218.81	16.08	0.67
Skjell-63	452.03	27	400000.19	12650.15	1080.42	210.11	16.29	0.69
Skjell-64	430.06	26.03	400000.19	12650.33	1077.75	209.71	11.45	0.49
Skjell-65	408.79	25.09	400000.22	12650.3	1006.72	196.02	11.68	0.5
Skjell-66	343.54	21.4	400000.19	12650.13	995.48	193.95	14.47	0.63

Skjell-67	363.99	23.01	400000.22	12650.12	1005.76	196.09	15.27	0.67
610-19	445.37	28.59	81475.99	2577.09	522.69	101.98	459.36	20.34
610-20	432.52	28.21	81475.99	2577.08	513.65	100.29	451.27	20.2
610-21	423.65	28.08	81476	2577.07	506.83	99.03	447.15	20.25
Skjell-68	333.09	22.44	400000.25	12650.05	1007.53	197.02	14.59	0.67
Skjell-69	424.7	29.1	400000.25	12650.12	1084.84	212.31	13.52	0.63
Skjell-70	396.21	27.61	400000.22	12650.14	1118.96	219.17	11.62	0.55
Skjell-71	423.36	30.01	400000.25	12650.08	1113.51	218.3	16.04	0.76
Skjell-72	357.4	25.77	400000.25	12650.07	1223.53	240.08	20.49	0.99
Skjell-73	328.77	24.12	400000.25	12650.08	1413.44	277.6	37.85	1.85
Skjell-74	345.99	25.83	400000.25	12650.03	1439.82	283.05	53.85	2.66
Skjell-75	855.69	65.01	400000.28	12650.11	1248.11	245.6	25.24	1.26
Skjell-76	568.12	43.92	400000.25	12650.17	1187.72	233.96	17.27	0.88
Skjell-77	398.3	31.34	400000.25	12650.18	1270.62	250.54	25.28	1.3
Skjell-78	563.85	45.15	400000.25	12650.18	1299.68	256.55	32.46	1.69
Skjell-79	823.26	67.08	400000.25	12651.1	1127.59	222.82	40.23	2.13
Skjell-80	729.77	60.51	400000.28	12650.72	1181.54	233.74	56.91	3.05
Skjell-81	840.73	70.95	400000.22	12655.23	1341.11	265.62	53.09	2.89
610-22	452.45	38.84	81476	2577.15	530.39	105.17	463.96	25.56
610-23	411.8	35.97	81476	2577.13	506.97	100.64	440.33	24.6
610-24	433.95	38.56	81476	2577.12	513.89	102.14	453.5	25.69

Appendix 2: Table of LA-ICPMS results used for diagrams, Skådalen

Results for LA-ICPMS analysis of *M. edulis* from the Skådalen locality used for diagrams. Added Ba/Ca (µmol/mol).

Results for LA-ICPMS of *M. edulis* shell from the Skådalen locality used for diagrams						
	Approximate distance from umbo (mm)	Mg (ppm)	Ca (ppm)	Sr (ppm)	Ba (ppm)	Ba/Ca (µmol/mol)
Skjell-01	0.5	840.73	400000.22	1341.11	53.09	38.7557
Skjell-02	1	729.77	400000.28	1181.54	56.91	41.5443
Skjell-03	1.5	823.26	400000.25	1127.59	40.23	29.3679
Skjell-04	2	563.85	400000.25	1299.68	32.46	23.6958
Skjell-05	2.5	398.3	400000.25	1270.62	25.28	18.4544
Skjell-06	3	568.12	400000.25	1187.72	17.27	12.6071
Skjell-07	3.5	855.69	400000.28	1248.11	25.24	18.4252
Skjell-08	4	345.99	400000.25	1439.82	53.85	39.3105
Skjell-09	4.5	328.77	400000.25	1413.44	37.85	27.6305
Skjell-10	5	357.4	400000.25	1223.53	20.49	14.9577
Skjell-11	5.5	423.36	400000.25	1113.51	16.04	11.7092
Skjell-12	6	396.21	400000.22	1118.96	11.62	8.4826
Skjell-13	6.5	424.7	400000.25	1084.84	13.52	9.8696
Skjell-14	7	333.09	400000.25	1007.53	14.59	10.6507
Skjell-15	7.5	363.99	400000.22	1005.76	15.27	11.1471
Skjell-16	8	343.54	400000.19	995.48	14.47	10.5631
Skjell-17	8.5	408.79	400000.22	1006.72	11.68	8.5264
Skjell-18	9	430.06	400000.19	1077.75	11.45	8.3585
Skjell-19	9.5	452.03	400000.19	1080.42	16.29	11.8917
Skjell-20	10	500.14	400000.19	1125.79	16.08	11.7384
Skjell-21	10.5	558.59	400000.19	1095.49	14.66	10.7018
Skjell-22	11	451.14	400000.22	1153.88	18.96	13.8408
Skjell-23	11.5	442.49	400000.22	1210.89	21.34	15.5782
Skjell-24	12	492.82	400000.19	1059.7	11.06	8.0738
Skjell-25	12.5	569.47	400000.19	1027.57	9.29	6.7817
Skjell-26	13	521.78	400000.19	1116.44	6.74	4.9202
Skjell-27	13.5	631.31	400000.22	1068.64	5.84	4.2632
Skjell-28	14	593.81	400000.19	1147.59	6.95	5.0735
Skjell-29	14.5	501.45	400000.19	1117.89	6.28	4.5844
Skjell-30	15	333.69	285880.44	780.99	4.35	3.1755
Skjell-31	15.5	587.99	400000.34	922.6	5.35	3.9055
Skjell-32	16	589.73	400000.34	1034.04	5.12	3.7376
Skjell-33	16.5	387.04	400000.38	1065.1	5.23	3.8179
Skjell-34	17	400.64	400000.34	983.38	6.36	4.6428
Skjell-35	17.5	504.4	400000.31	1023.52	4.16	3.0368

Skjell-36	18	501.84	400000.34	1022.57	5.75	4.1975
Skjell-37	18.5	618.23	400000.34	1189.34	5.35	3.9055
Skjell-38	19	550.14	400000.31	1127.25	8.64	6.3072
Skjell-39	19.5	623.16	400000.34	1098.94	33.51	24.4623
Skjell-40	20	617.48	400000.34	1150.22	161.29	117.7417
Skjell-41	20.5	552.35	400000.31	1179.86	171.18	124.9614
Skjell-42	21	777.99	400000.34	1054.35	33.13	24.1849
Skjell-43	21.5	583.23	400000.31	1122.3	18.02	13.1546
Skjell-44	22	448.76	400000.34	1110.23	8.31	6.0663
Skjell-45	22.5	461.97	400000.31	1190.13	7.77	5.6721
Skjell-46	23	385.43	400000.31	1210.35	5.9	4.307
Skjell-47	23.5	430.01	400000.34	1076.14	6.96	5.0808
Skjell-48	24	405	400000.34	1089	7.53	5.4969
Skjell-49	24.5	314.36	400000.34	1221.63	25.8	18.834
Skjell-50	25	371.84	400000.34	1104.51	14	10.22
Skjell-51	25.5	540.64	400000.34	1135.64	26	18.98
Skjell-52	26	765.09	400000.31	1449.31	45.12	32.9376
Skjell-53	26.5	780.42	400000.31	1559.28	60.88	44.4424
Skjell-54	27	597.99	400000.31	1456.43	26.62	19.4326
Skjell-55	27.5	606.31	400000.31	1471.83	14.92	10.8916
Skjell-56	28	585.58	400000.31	1440.99	9.65	7.0445
Skjell-57	28.5	396.84	400000.31	1255.87	7.51	5.4823
Skjell-58	29	514.09	400000.28	1150.75	6.58	4.8034
Skjell-59	29.5	452.92	400000.31	1127.52	6.52	4.7596
Skjell-60	30	541.31	400000.28	1184.53	12.69	9.2637
Skjell-61	30.5	701.41	400000.31	1369.76	20.84	15.2132
Skjell-62	31	768.15	400000.31	1288.21	7.45	5.4385
Skjell-63	31.5	1034.56	400000.31	1429.82	12.99	9.4827
Skjell-64	32	812.54	400000.31	1327.21	12.82	9.3586
Skjell-65	32.5	810.86	400000.28	1310.49	11.14	8.1322
Skjell-66	33	887.13	400000.28	1355.06	14.6	10.658
Skjell-67	33.5	558.64	400000.28	1313.88	10.53	7.6869
Skjell-68	34	883.15	400000.28	1178.51	13.27	9.6871
Skjell-69	34.5	705.8	400000.28	1316.71	15.5	11.315
Skjell-70	35	1175.22	400000.28	1517.75	20.79	15.1767
Skjell-71	35.5	561.16	400000.28	1255.68	16.25	11.8625
Skjell-72	36	601.26	400000.28	1189.29	20.43	14.9139
Skjell-73	36.5	632.09	400000.28	1352.33	23.44	17.1112
Skjell-74	37	711.88	400000.28	1247.3	19.53	14.2569
Skjell-75	37.5	450.69	400000.28	1389.07	25.26	18.4398
Skjell-76	38	418.99	400000.28	1482.86	26.39	19.2647
Skjell-77	38.5	530.5	400000.25	1114.07	9.7	7.081
Skjell-78	39	522.31	400000.25	1116.97	14.09	10.2857
Skjell-79	39.5	635.98	400000.25	1159.27	12.68	9.2564
Skjell-80	40	821.1	400000.25	1322.22	16.55	12.0815
Skjell-81	40.5	1116.9	400000.25	1337.49	17.3	12.629

Appendix 3: Table of LA-ICPMS results for Sognsvann

Results for LA-ICPMS analysis for *M. edulis* for the Sognsvann locality.

Results for LA-ICPMS of *M. edulis* shell from the Sognsvann locality								
	Mg (ppm)	1sigma	Ca (ppm)	1sigma	Sr (ppm)	1sigma	Ba (ppm)	1sigma
610-01	380	65.47	81476.03	2576.97	526.38	170.2	475.31	28.58
610-02	368.98	63.38	81476.03	2576.97	514.2	166.21	460.82	27.71
610-03	357.94	61.31	81476.04	2576.96	502.36	162.32	447.26	26.88
Skjell-01	29.85	5.16	400000.38	12650.19	1440.8	465.39	13.75	0.83
Skjell-02	38.72	6.66	400000.41	12650.38	1352.26	436.64	14.59	0.88
Skjell-03	32.5	5.6	400000.38	12650.41	1888.33	609.53	11.5	0.69
Skjell-04	29.46	5.07	400000.38	12650.38	2130.6	687.49	20.82	1.25
Skjell-05	32.16	5.51	400000.41	12650.44	1735.43	559.79	16.32	0.98
Skjell-06	31.69	5.41	400000.41	12650.41	1609.58	519.03	15.18	0.92
Skjell-07	27.16	4.67	400000.41	12650.58	2139.33	689.62	22.71	1.37
Skjell-08	28.53	4.88	400000.41	12650.56	2183.18	703.52	19.16	1.16
Skjell-09	24.17	4.18	400000.41	12650.74	1383.39	445.64	9.08	0.55
Skjell-10	21.83	3.78	400000.41	12650.64	1260.43	405.9	6.82	0.42
Skjell-11	28.65	4.85	400000.41	12650.39	1151.44	370.68	5.77	0.35
Skjell-12	35.36	5.95	400000.41	12650.49	1547.06	497.89	13.72	0.83
Skjell-13	34.79	5.86	400000.38	12650.57	1613.25	519.02	15.6	0.94
Skjell-14	33.95	5.71	400000.38	12650.52	1759.11	565.77	17.5	1.06
Skjell-15	39.62	6.62	400000.41	12650.41	2518.17	809.64	19.87	1.2
610-04	433.05	71.68	81476.03	2577.12	514.89	165.49	447.75	27.05
610-05	426.58	70.51	81476.03	2577.1	511.54	164.37	445.28	26.92
610-06	423.89	69.97	81476.03	2577.13	508.51	163.34	445.03	26.93
Skjell-16	41.51	6.91	400000.41	12651.01	2457.16	789.04	21.11	1.28
Skjell-17	44.53	7.37	400000.41	12650.48	2471.05	793.25	19.59	1.19
Skjell-18	48.15	8	400000.38	12651.24	2114.93	678.73	22.65	1.38
Skjell-19	42.06	6.95	400000.41	12650.35	2332.02	748.17	27.99	1.7
Skjell-20	48.37	7.98	400000.38	12650.41	2478.51	794.93	26.79	1.63
Skjell-21	45.18	7.45	400000.41	12650.47	2490.13	798.42	19.9	1.21
Skjell-22	39.78	6.57	400000.41	12650.53	2353.18	754.29	15.51	0.95
Skjell-23	31.39	5.2	400000.41	12650.58	1648.93	528.39	9.54	0.59
Skjell-24	25.8	4.29	400000.41	12650.65	1271.08	407.2	7.57	0.47
Skjell-25	26.35	4.37	400000.41	12650.56	1439.56	461.03	8	0.49
Skjell-26	25.15	4.18	400000.41	12650.48	1396.16	447.01	7.75	0.48
Skjell-27	22.01	3.68	400000.38	12650.7	1214.59	388.77	7.51	0.47
Skjell-28	23.14	3.87	400000.38	12650.75	1246.4	398.83	7.2	0.45
Skjell-29	34.29	5.65	400000.41	12650.56	1994.64	638.08	12.24	0.76
610-07	463.48	75.69	81476.03	2577.19	510.3	163.2	443.03	27.34
610-08	455.35	74.36	81476.03	2577.18	505.25	161.54	438.66	27.12
610-09	450.78	73.6	81476.03	2577.22	502.12	160.5	437.67	27.1

Skjell-30	31.56	5.23	400000.41	12651.09	2053.85	656.3	12.64	0.79
Skjell-31	29.64	4.9	400000.38	12650.63	1835.53	586.38	10.33	0.65
Skjell-32	21.64	3.62	400000.41	12650.7	1284.1	410.11	6.05	0.38
Skjell-33	25.64	4.26	400000.41	12650.61	1367.55	436.65	6.83	0.43
Skjell-34	39.83	6.56	400000.41	12650.8	1967.15	627.93	15.39	0.97
Skjell-35	38.1	6.27	400000.41	12650.66	1855.74	592.21	10.33	0.65
Skjell-36	29.3	4.85	400000.38	12650.73	1257.35	401.15	6.42	0.41
Skjell-37	32.37	5.35	400000.38	12650.7	1308.64	417.4	6.56	0.42
Skjell-38	30.4	5.03	400000.38	12650.64	1265.45	403.52	6.69	0.43
Skjell-39	36.92	6.09	400000.38	12650.59	1511.31	481.8	7.46	0.48
Skjell-40	25.88	4.3	400000.38	12650.59	1274.78	406.29	6.67	0.43
Skjell-41	26.96	4.48	400000.41	12650.6	1264.45	402.9	6.78	0.44
Skjell-42	29.23	4.85	400000.41	12650.68	1286.25	409.75	6.42	0.41
Skjell-43	27.12	4.51	400000.38	12650.6	1228.81	391.35	6.08	0.39
Skjell-44	28.36	4.71	400000.38	12650.63	1194.33	380.28	5.93	0.38
Skjell-45	30.21	5.01	400000.38	12650.59	1190.8	379.07	5.93	0.39
610-12	461.58	75.96	81475.94	2577.27	500.88	159.41	436.44	28.03
610-12	460.35	75.83	81476.03	2577.27	500.7	159.31	436.27	28.09
610-11	463.03	76.34	81476.03	2577.22	504.94	160.62	437.24	28.23
610-10	468.98	77.4	81476.03	2577.24	510.37	162.32	444.71	28.78
Skjell-46	29.77	4.97	400000.41	12650.54	1136.71	361.42	7.32	0.48
Skjell-47	26.7	4.47	400000.38	12650.62	1285.65	408.69	6.46	0.43
Skjell-48	33.26	5.55	400000.38	12650.54	1356.74	431.19	7.38	0.49
Skjell-49	31.08	5.2	400000.41	12650.56	1302.19	413.76	9.09	0.6
Skjell-50	30.24	5.07	400000.41	12650.71	1455.15	462.26	13.75	0.91
Skjell-51	30.56	5.13	400000.41	12651.38	1399.17	444.38	15.28	1.01
Skjell-52	30.94	5.2	400000.38	12650.76	1857.99	589.97	21.44	1.42
Skjell-53	31.5	5.29	400000.38	12650.68	1752.92	556.49	19.75	1.31
Skjell-54	35.11	5.9	400000.38	12650.74	1499.86	476.05	16.35	1.09
Skjell-55	33.32	5.61	400000.41	12650.71	1719.82	545.75	21.65	1.44
Skjell-56	38.46	6.47	400000.41	12650.71	2012.32	638.44	23.7	1.58
Skjell-57	25.24	4.27	400000.38	12650.57	1628.94	516.7	8.69	0.59
Skjell-58	27.7	4.7	400000.41	12650.76	1381.2	438.03	7.44	0.5
Skjell-59	31.25	5.3	400000.41	12650.86	1391.95	441.35	7.22	0.49
Skjell-60	39.07	6.61	400000.38	12650.64	1418	449.51	7.17	0.49
610-13	475.05	80.1	81476.03	2577.2	520.89	165.09	452.14	30.62
610-14	467.49	78.96	81476.03	2577.25	512.54	162.42	444.15	30.17
610-15	459.37	77.71	81476.03	2577.26	506.57	160.49	441.48	30.08
Skjell-61	39.15	6.66	400000.38	12650.59	1388.51	439.82	6.81	0.47
Skjell-62	39.49	6.74	400000.38	12650.71	1345.6	426.15	7.28	0.5
Skjell-63	34.29	5.87	400000.41	12650.7	1382.59	437.78	7.18	0.5
Skjell-64	36.6	6.26	400000.41	12650.64	1404.37	444.6	7.23	0.5
Skjell-65	33.52	5.75	400000.38	12650.6	1533.75	485.47	8.22	0.57
Skjell-66	37.66	6.47	400000.38	12650.61	1501.53	475.18	7.71	0.54
Skjell-67	36.86	6.34	400000.41	12650.68	1469.63	465	7.27	0.51
Skjell-68	38.36	6.61	400000.38	12650.65	1417.23	448.34	8.28	0.58

Skjell-69	42.84	7.39	400000.38	12650.65	1691.66	535.07	15.7	1.1
Skjell-70	34.24	5.94	400000.38	12650.88	1500.44	474.5	9.36	0.66
Skjell-71	37.8	6.59	400000.38	12651.66	1704.43	538.92	15.76	1.12
Skjell-72	47.19	8.19	400000.41	12651.12	2498.43	789.84	25.45	1.8
Skjell-73	36.53	6.36	400000.41	12650.72	1918.81	606.5	17.74	1.26
Skjell-74	33.56	5.87	400000.38	12651.06	1904.74	601.96	15.1	1.08
Skjell-75	39.6	6.92	400000.41	12650.98	2113.37	667.78	18.93	1.36
610-16	480.2	83.66	81476.03	2577.23	538.63	170.17	468.31	33.59
610-17	470.73	82.17	81476.03	2577.27	525.93	166.13	457.25	32.91
610-18	466.43	81.58	81476.02	2577.23	519.52	164.08	452.67	32.69
Skjell-76	29.71	5.28	400000.38	12651.52	1587.75	501.38	8.61	0.63
Skjell-77	32.41	5.73	400000.44	12650.99	1657.56	523.34	10.48	0.77
Skjell-78	40.82	7.21	400000.38	12650.86	2147.06	677.79	21.43	1.57
Skjell-79	45.53	8.06	400000.41	12650.88	2356.53	743.8	24.32	1.78
Skjell-80	29.42	5.23	400000.41	12650.76	1747.18	551.39	9.49	0.7
Skjell-81	25.06	4.49	400000.41	12650.97	1696.11	535.2	7.82	0.58
Skjell-82	31.97	5.71	400000.38	12651.07	2217.03	699.47	11.88	0.88
Skjell-83	24.2	4.37	400000.41	12651.4	1863.14	587.74	8.22	0.62
Skjell-84	26.73	4.82	400000.41	12651.24	1755.79	553.8	8.18	0.62
Skjell-85	21.49	3.91	400000.38	12651.37	1769.84	558.15	8.46	0.64
Skjell-86	27.05	4.91	400000.38	12651.82	1786.54	563.34	8.52	0.65
Skjell-87	27.94	5.06	400000.34	12651.25	1713.73	540.31	7.8	0.59
Skjell-88	37.5	6.77	400000.41	12650.82	1932.24	609.12	13.49	1.02
Skjell-89	31.62	5.73	400000.41	12650.94	1785.34	562.74	9.37	0.71
Skjell-90	56.4	10.2	400000.34	12651.06	2586.75	815.24	26.94	2.05
610-19	474.91	85.9	81476.03	2577.24	549.92	173.29	482.98	36.86
610-20	464.52	84.21	81476.03	2577.26	535.14	168.61	468.65	35.89
610-21	458.98	83.38	81476.02	2577.3	529.33	166.76	463.24	35.6
Skjell-91	75.93	13.84	400000.41	12650.89	3541.92	1115.72	29.54	2.28
Skjell-92	82.56	15.08	400000.38	12650.66	3446.77	1085.62	24.53	1.9
Skjell-93	78.27	14.33	400000.41	12650.79	3516.4	1107.43	25.02	1.95
Skjell-94	79.2	14.53	400000.41	12650.72	3447.87	1085.72	27.81	2.17
Skjell-95	69.57	12.79	400000.41	12650.88	3345.02	1053.22	32.62	2.55
Skjell-96	80.27	14.79	400000.41	12650.89	3440.32	1083.11	31.55	2.48
Skjell-97	65.5	12.1	400000.41	12651.01	3228.06	1016.17	31.49	2.48
Skjell-98	70.81	13.11	400000.44	12650.97	3243.04	1020.78	31.21	2.47
Skjell-99	38.21	7.1	400000.41	12650.78	2081.65	655.16	22.43	1.78
Skjell-100	85.47	15.89	400000.38	12650.99	3390.71	1067.05	29.01	2.31
Skjell-101	56.15	10.47	400000.41	12650.82	2729.21	858.79	29.48	2.36
Skjell-102	63.21	11.8	400000.41	12650.71	3006.55	945.97	30.34	2.43
Skjell-103	74.58	13.95	400000.41	12650.9	3345.18	1052.41	31.2	2.51
Skjell-104	62.58	11.74	400000.44	12650.87	3151.9	991.51	31.64	2.56
Skjell-105	58.99	11.09	400000.41	12650.86	3061.82	963.09	31.82	2.58
610-22	461.74	86.89	81476.03	2577.26	547.55	172.22	479.13	38.96
610-23	453.35	85.5	81476.03	2577.26	532.5	167.47	464.71	37.92
610-24	447	84.49	81476.03	2577.27	523.88	164.74	457.12	37.44

Skjell-106	79.2	15.02	400000.41	12650.89	3147.11	989.57	26.82	2.21
Skjell-107	79.72	15.15	400000.41	12650.86	3135.54	985.85	31.93	2.64
Skjell-108	77.78	14.81	400000.38	12650.74	3336.94	1049.09	26.79	2.22
Skjell-109	73.2	13.97	400000.38	12650.77	3382.45	1063.31	26.54	2.21
Skjell-110	117.8	22.52	400000.41	12650.95	3170.14	996.5	68.13	5.68
Skjell-111	59.44	11.43	400000.38	12652.38	2961.56	930.87	33.75	2.83
Skjell-112	150.41	28.89	400000.41	12652.4	3468.81	1090.22	40.45	3.4
Skjell-113	708.38	136.28	400000.41	12650.89	1034.85	325.23	1.31	0.13
Skjell-114	80.07	15.46	400000.38	12651.47	3474.67	1091.91	39.8	3.37
Skjell-115	344.3	66.53	400000.38	12650.99	2967.05	932.33	38.63	3.28
Skjell-116	50.1	9.72	400000.38	12651.11	3140.87	986.89	22.37	1.91
Skjell-117	62.69	12.18	400000.38	12651.22	3376.15	1060.75	27.45	2.35
Skjell-118	528.07	102.72	400000.38	12651.39	2482.39	779.89	17.69	1.52
Skjell-119	394.9	76.98	400000.38	12651.2	3144.29	987.78	22.96	1.98
Skjell-120	944.88	184.59	400000.41	12651.55	1653.13	519.31	14.7	1.27
610-25	445.65	87.25	81476.03	2577.29	536.25	168.44	471.33	40.84
610-26	435.5	85.45	81476.03	2577.26	521.86	163.92	457.74	39.81
610-27	429.25	84.41	81476.03	2577.27	514.74	161.67	451.61	39.41
Skjell-121	1133.53	223.38	400000.38	12651.56	1524.07	478.67	14.04	1.23
Skjell-122	479.83	94.77	400000.41	12651.86	3184.17	1000	34.9	3.07
Skjell-123	1034.66	204.79	400000.41	12651.8	1908.01	599.19	21.12	1.87
Skjell-124	160.51	31.95	400000.41	12659.78	3843.7	1207.04	44.22	3.93
Skjell-125	203.67	40.5	400000.38	12652.24	3200.39	1004.96	25.42	2.26
Skjell-126	513.6	102.32	400000.44	12650.95	1210.49	380.1	3.13	0.29
Skjell-127	568.77	113.55	400000.41	12651.01	1336.29	419.58	4.76	0.43
Skjell-128	627.43	125.53	400000.41	12652	1319.96	414.44	4.12	0.38
Skjell-129	653.6	131.05	400000.41	12650.9	1106.3	347.34	1.82	0.17
Skjell-130	688.79	138.39	400000.41	12650.73	1140.98	358.22	2.17	0.2
Skjell-131	626.99	126.25	400000.44	12650.85	1103.59	346.47	2.43	0.23
Skjell-132	645.68	130.29	400000.38	12650.86	1123.18	352.61	2.13	0.2
Skjell-133	644	130.23	400000.41	12651.31	969.16	304.25	5.37	0.5
Skjell-134	902.41	182.86	400000.38	12651.03	1240.53	389.43	16.93	1.55
Skjell-135	678.92	137.87	400000.41	12650.8	1064.52	334.17	3	0.28
610-28	428.83	87.27	81476.03	2577.28	530.93	166.66	467.96	43.17
610-29	420.43	85.74	81476.03	2577.29	516.53	162.14	452.98	41.93
610-30	414.83	84.77	81476.03	2577.28	508.35	159.57	445.34	41.36
Skjell-136	658.68	134.89	400000.38	12650.68	1006.33	315.88	2.82	0.27
Skjell-137	807.93	165.79	400000.41	12650.74	1149.71	360.88	9.13	0.86
Skjell-138	997.29	205.08	400000.41	12650.81	1309.22	410.94	14.83	1.39
Skjell-139	903.35	186.15	400000.38	12652	1185.31	372.05	10.69	1.01
Skjell-140	966.08	199.48	400000.34	12650.68	1118.41	351.04	3.62	0.35
Skjell-141	835.45	172.87	400000.38	12650.77	1088.8	341.75	2.59	0.25
Skjell-142	1226.96	254.4	400000.41	12650.63	1153.21	361.96	5.14	0.49
Skjell-143	1258.73	261.52	400000.34	12650.64	1200.75	376.88	5.75	0.55
Skjell-144	478.03	99.53	400000.34	12652.77	910.64	285.83	2.43	0.26
Skjell-145	918.69	191.66	400000.38	12650.98	1012.46	317.78	3.99	0.39

Skjell-146	551.8	115.35	400000.38	12651.03	959.4	301.13	2.02	0.2
Skjell-147	780.02	163.39	400000.34	12650.76	1105.15	346.88	5.26	0.51
Skjell-148	798.06	167.51	400000.34	12650.72	1119.21	351.29	5.79	0.56
Skjell-149	1203.17	253.05	400000.38	12650.76	1151.91	361.56	9.87	0.96
Skjell-150	557.39	117.47	400000.34	12651.56	821.58	257.88	1.92	0.21
610-31	412.25	87.05	81476.02	2577.25	518.09	162.62	456.03	44.7
610-32	404.88	85.67	81476.02	2577.25	503.14	157.93	442.66	43.53
610-33	398.84	84.56	81476.02	2577.28	496.91	155.98	437.42	43.16
Skjell-151	519.97	110.46	400000.38	12651	795.14	249.6	2.07	0.22
Skjell-152	506.61	107.84	400000.38	12650.91	889.37	279.18	2.13	0.22
Skjell-153	567.33	121	400000.34	12650.92	900.46	282.66	2.72	0.28
Skjell-154	516.75	110.43	400000.38	12651.09	881.17	276.61	2.89	0.3
Skjell-155	462.97	99.13	400000.38	12651.27	931.86	292.53	2.68	0.28
Skjell-156	432.62	92.81	400000.34	12650.67	1010.43	317.21	4.25	0.43
610-34	401.22	86.24	81476.02	2577.31	503.74	158.14	446.05	45.03
610-35	390.66	84.14	81476.02	2577.3	489.4	153.65	434.15	43.97
610-36	386.3	83.36	81476.03	2577.33	483.5	151.8	430.08	43.7

Appendix 4: Table of LA-ICPMS results used for diagrams, Sognsvann

Results for LA-ICPMS analysis of *M. edulis* from the Sognsvann locality used for diagrams. Added Ba/Ca (µmol/mol).

Results for LA-ICPMS of *M. edulis* shell from the Sognsvann locality used for diagrams						
	Approximate distance from umbo (mm)	Mg (ppm)	Ca (ppm)	Sr (ppm)	Ba (ppm)	Ba/Ca (µmol/mol)
Skjell-01	0.5	29.85	400000.38	1440.8	13.75	10.0375
Skjell-02	1	38.72	400000.41	1352.26	14.59	10.6507
Skjell-03	1.5	32.5	400000.38	1888.33	11.5	8.395
Skjell-04	2	29.46	400000.38	2130.6	20.82	15.1986
Skjell-05	2.5	32.16	400000.41	1735.43	16.32	11.9136
Skjell-06	3	31.69	400000.41	1609.58	15.18	11.0814
Skjell-07	3.5	27.16	400000.41	2139.33	22.71	16.5783
Skjell-08	4	28.53	400000.41	2183.18	19.16	13.9868
Skjell-09	4.5	24.17	400000.41	1383.39	9.08	6.6284
Skjell-10	5	21.83	400000.41	1260.43	6.82	4.9786
Skjell-11	5.5	28.65	400000.41	1151.44	5.77	4.2121
Skjell-12	6	35.36	400000.41	1547.06	13.72	10.0156
Skjell-13	6.5	34.79	400000.38	1613.25	15.6	11.388
Skjell-14	7	33.95	400000.38	1759.11	17.5	12.775
Skjell-15	7.5	39.62	400000.41	2518.17	19.87	14.5051
Skjell-16	8	41.51	400000.41	2457.16	21.11	15.4103
Skjell-17	8.5	44.53	400000.41	2471.05	19.59	14.3007
Skjell-18	9	48.15	400000.38	2114.93	22.65	16.5345
Skjell-19	9.5	42.06	400000.41	2332.02	27.99	20.4327
Skjell-20	10	48.37	400000.38	2478.51	26.79	19.5567
Skjell-21	10.5	45.18	400000.41	2490.13	19.9	14.527
Skjell-22	11	39.78	400000.41	2353.18	15.51	11.3223
Skjell-23	11.5	31.39	400000.41	1648.93	9.54	6.9642
Skjell-24	12	25.8	400000.41	1271.08	7.57	5.5261
Skjell-25	12.5	26.35	400000.41	1439.56	8	5.84
Skjell-26	13	25.15	400000.41	1396.16	7.75	5.6575
Skjell-27	13.5	22.01	400000.38	1214.59	7.51	5.4823
Skjell-28	14	23.14	400000.38	1246.4	7.2	5.256
Skjell-29	14.5	34.29	400000.41	1994.64	12.24	8.9352
Skjell-30	15	31.56	400000.41	2053.85	12.64	9.2272
Skjell-31	15.5	29.64	400000.38	1835.53	10.33	7.5409
Skjell-32	16	21.64	400000.41	1284.1	6.05	4.4165
Skjell-33	16.5	25.64	400000.41	1367.55	6.83	4.9859

Skjell-34	17	39.83	400000.41	1967.15	15.39	11.2347
Skjell-35	17.5	38.1	400000.41	1855.74	10.33	7.5409
Skjell-36	18	29.3	400000.38	1257.35	6.42	4.6866
Skjell-37	18.5	32.37	400000.38	1308.64	6.56	4.7888
Skjell-38	19	30.4	400000.38	1265.45	6.69	4.8837
Skjell-39	19.5	36.92	400000.38	1511.31	7.46	5.4458
Skjell-40	20	25.88	400000.38	1274.78	6.67	4.8691
Skjell-41	20.5	26.96	400000.41	1264.45	6.78	4.9494
Skjell-42	21	29.23	400000.41	1286.25	6.42	4.6866
Skjell-43	21.5	27.12	400000.38	1228.81	6.08	4.4384
Skjell-44	22	28.36	400000.38	1194.33	5.93	4.3289
Skjell-45	22.5	30.21	400000.38	1190.8	5.93	4.3289
Skjell-46	23	29.77	400000.41	1136.71	7.32	5.3436
Skjell-47	23.5	26.7	400000.38	1285.65	6.46	4.7158
Skjell-48	24	33.26	400000.38	1356.74	7.38	5.3874
Skjell-49	24.5	31.08	400000.41	1302.19	9.09	6.6357
Skjell-50	25	30.24	400000.41	1455.15	13.75	10.0375
Skjell-51	25.5	30.56	400000.41	1399.17	15.28	11.1544
Skjell-52	26	30.94	400000.38	1857.99	21.44	15.6512
Skjell-53	26.5	31.5	400000.38	1752.92	19.75	14.4175
Skjell-54	27	35.11	400000.38	1499.86	16.35	11.9355
Skjell-55	27.5	33.32	400000.41	1719.82	21.65	15.8045
Skjell-56	28	38.46	400000.41	2012.32	23.7	17.301
Skjell-57	28.5	25.24	400000.38	1628.94	8.69	6.3437
Skjell-58	29	27.7	400000.41	1381.2	7.44	5.4312
Skjell-59	29.5	31.25	400000.41	1391.95	7.22	5.2706
Skjell-60	30	39.07	400000.38	1418	7.17	5.2341
Skjell-61	30.5	39.15	400000.38	1388.51	6.81	4.9713
Skjell-62	31	39.49	400000.38	1345.6	7.28	5.3144
Skjell-63	31.5	34.9	400000.41	1382.59	7.18	5.2414
Skjell-64	32	36.6	400000.41	1404.37	7.23	5.2779
Skjell-65	32.5	33.52	400000.38	1533.75	8.22	6.0006
Skjell-66	33	37.66	400000.38	1501.53	7.71	5.6283
Skjell-67	33.5	36.86	400000.41	1469.63	7.27	5.3071
Skjell-68	34	38.36	400000.38	1417.23	8.28	6.0444
Skjell-69	34.5	42.84	400000.38	1691.66	15.7	11.461
Skjell-70	35	34.24	400000.38	1500.44	9.36	6.8328
Skjell-71	35.5	37.8	400000.38	1704.43	15.76	11.5048
Skjell-72	36	47.19	400000.41	2498.43	25.45	18.5785
Skjell-73	36.5	36.53	400000.41	1918.81	17.74	12.9502
Skjell-74	37	33.56	400000.38	1904.74	15.1	11.023
Skjell-75	37.5	39.6	400000.41	2113.37	18.93	13.8189
Skjell-76	38	29.71	400000.38	1587.75	8.61	6.2853
Skjell-77	38.5	32.41	400000.44	1657.56	10.48	7.6504
Skjell-78	39	40.82	400000.38	2147.06	21.43	15.6439
Skjell-79	39.5	45.53	400000.41	2356.53	24.32	17.7536

Skjell-80	40	29.42	400000.41	1747.18	9.49	6.9277
Skjell-81	40.5	25.06	400000.41	1696.11	7.82	5.7086
Skjell-82	41	31.97	400000.38	2217.03	11.88	8.6724
Skjell-83	41.5	24.2	400000.41	1863.14	8.22	6.0006
Skjell-84	42	26.73	400000.41	1755.79	8.18	5.9714
Skjell-85	42.5	21.49	400000.38	1769.84	8.46	6.1758
Skjell-86	43	27.05	400000.38	1786.54	8.52	6.2196
Skjell-87	43.5	27.94	400000.34	1713.73	7.8	5.694
Skjell-88	44	37.5	400000.41	1932.24	13.49	9.8477
Skjell-89	44.5	31.62	400000.41	1785.34	9.37	6.8401
Skjell-90	45	56.4	400000.34	2586.75	26.94	19.6662
Skjell-91	45.5	75.93	400000.41	3541.92	29.54	21.5642
Skjell-92	46	82.56	400000.38	3446.77	24.53	17.9069
Skjell-93	46.5	78.27	400000.41	3516.4	25.02	18.2646
Skjell-94	47	79.2	400000.41	3447.87	27.81	20.3013
Skjell-95	47.5	69.57	400000.41	3345.02	32.62	23.8126
Skjell-96	48	80.27	400000.41	3440.32	31.55	23.0315
Skjell-97	48.5	65.5	400000.41	3228.06	31.49	22.9877
Skjell-98	49	70.81	400000.44	3243.04	31.21	22.7833
Skjell-99	49.5	38.21	400000.41	2081.65	22.43	16.3739
Skjell-100	50	85.47	400000.38	3390.71	29.01	21.1773
Skjell-101	50.5	56.15	400000.41	2729.21	29.48	21.5204
Skjell-102	51	63.21	400000.41	3006.55	30.34	22.1482
Skjell-103	51.5	74.58	400000.41	3345.18	31.2	22.776
Skjell-104	52	62.58	400000.44	3151.9	31.64	23.0972
Skjell-105	52.5	58.99	400000.41	3061.82	31.82	23.2286
Skjell-106	53	79.2	400000.41	3147.11	26.82	19.5786
Skjell-107	53.5	79.72	400000.41	3135.54	31.93	23.3089
Skjell-108	54	77.78	400000.38	3336.94	26.79	19.5567
Skjell-109	54.5	73.2	400000.38	3382.45	26.54	19.3742
Skjell-110	55	117.8	400000.41	3170.14	68.13	49.7349
Skjell-111	55.5	59.44	400000.38	2961.56	33.75	24.6375
Skjell-112	56	150.41	400000.41	3468.81	40.45	29.5285
Skjell-113	56.5	708.38	400000.41	1034.85	1.31	0.9563
Skjell-114	57	80.07	400000.38	3474.67	39.8	29.054
Skjell-115	57.5	344.3	400000.38	2967.05	38.63	28.1999
Skjell-116	58	50.1	400000.38	3140.87	22.37	16.3301
Skjell-117	58.5	62.69	400000.38	3376.15	27.45	20.0385
Skjell-118	59	528.07	400000.38	2482.39	17.69	12.9137
Skjell-119	59.5	394.9	400000.38	3144.29	22.96	16.7608
Skjell-120	60	944.88	400000.41	1653.13	14.7	10.731
Skjell-121	60.5	1133.53	400000.38	1524.07	14.04	10.2492
Skjell-122	61	479.83	400000.41	3184.17	34.9	25.477
Skjell-123	61.5	1034.66	400000.41	1908.01	21.12	15.4176
Skjell-124	62	160.51	400000.41	3843.7	44.22	32.2806
Skjell-125	62.5	203.67	400000.38	3200.39	25.42	18.5566

Skjell-126	63	513.6	400000.44	1210.49	3.13	2.2849
Skjell-127	63.5	568.77	400000.41	1336.29	4.76	3.4748
Skjell-128	64	627.43	400000.41	1319.96	4.12	3.0076
Skjell-129	64.5	653.6	400000.41	1106.3	1.82	1.3286
Skjell-130	65	688.79	400000.41	1140.98	2.17	1.5841
Skjell-131	65.5	626.99	400000.44	1103.59	2.43	1.7739
Skjell-132	66	645.68	400000.38	1123.18	2.13	1.5549
Skjell-133	66.5	644	400000.41	969.16	5.37	3.9201
Skjell-134	67	902.41	400000.38	1240.53	16.93	12.3589
Skjell-135	67.5	678.92	400000.41	1064.52	3	2.19
Skjell-136	68	658.68	400000.38	1006.33	2.82	2.0586
Skjell-137	68.5	807.93	400000.41	1149.71	9.13	6.6649
Skjell-138	69	997.29	400000.41	1309.22	14.83	10.8259
Skjell-139	69.5	903.35	400000.38	1185.31	10.69	7.8037
Skjell-140	70	966.08	400000.34	1118.41	3.62	2.6426
Skjell-141	70.5	835.45	400000.38	1088.8	2.59	1.8907
Skjell-142	71	1226.96	400000.41	1153.21	5.14	3.7522
Skjell-143	71.5	1258.73	400000.34	1200.75	5.75	4.1975
Skjell-144	72	478.03	400000.34	910.64	2.43	1.7739
Skjell-145	72.5	918.69	400000.38	1012.46	3.99	2.9127
Skjell-146	73	551.8	400000.38	959.4	2.02	1.4746
Skjell-147	73.5	780.02	400000.34	1105.15	5.26	3.8398
Skjell-148	74	798.06	400000.34	1119.21	5.79	4.2267
Skjell-149	74.5	1203.17	400000.38	1151.91	9.87	7.2051
Skjell-150	75	557.39	400000.34	821.58	1.92	1.4016
Skjell-151	75.5	519.97	400000.38	795.14	2.07	1.5111
Skjell-152	76	506.61	400000.38	889.37	2.13	1.5549
Skjell-153	76.5	567.33	400000.34	900.46	2.72	1.9856
Skjell-154	77	516.75	400000.38	881.17	2.89	2.1097
Skjell-155	77.5	462.97	400000.38	931.86	2.68	1.9564
Skjell-156	78	432.62	400000.34	1010.43	4.25	3.1025

Appendix 5: Table of results for isotope analysis

Exernal precision (1-sigms standard deviation of the >240 standards run over the same period) is 0.03 and 0.06‰ for C and O isotopes respectively					
MYTILUS SHELL SAMPLES. SKÅDALEN. OSLO					
Sample #	**Identifier 1**	**FARLAB ID**	**d13C (VPDB)**	**d18O (VPDB)**	**Approximate distance from umbo (mm)**
J	J-1	2019-36-055	-2.16	-4.43	3
I	I-1	2019-36-054	-1.31	-1.55	6
H	H-1	2019-36-053	-1.11	-3.27	10
G	G-1	2019-36-052	-0.83	-0.30	13
F	F-1	2019-36-051	-0.64	-3.05	17
E	E-1	2019-36-050	-0.36	-1.52	20
D	D-1	2019-36-049	-1.06	-1.92	23
C	C-1	2019-36-048	-0.83	-0.89	27
B	B-1	2019-36-047	0.21	-3.23	30
A	A-1	2019-36-046	-2.01	-3.87	34

Appendix 6: Table of species

Species are listed in alphabetical order within each higher class. The list is based on the World Register of Marine Species (WoRMS Editorial Board, 2020).

Species name	Higher classification
Balanus balanus (Linnaeus, 1758)	Arthropoda, Crustacea
Cythere lutea Muller, 1785	Arthropoda, Crustacea
Sarsicytheridea bradii (Norman, 1865)	Arthropoda, Crustacea
Sarsicytheridea punctillata (Brady, 1865)	Arthropoda, Crustacea
Ophiura sarsii Lütken, 1855	Echinodermata, Ophiuroidea
Ammonia beccarii (Linnaeus, 1758)	Foraminifera, Globothalamea
Bulimina marginata d'Orbigny, 1826	Foraminifera, Globothalamea
Cassidulina teretis Tappan, 1951	Foraminifera, Globothalamea
Cribroelphidium incertum (Williamson, 1858)	Foraminifera, Globothalamea
Eggerelloides scaber (Williamson, 1858)	Foraminifera, Globothalamea
Elphidium excavatum subsp. clavatum Cushman, 1930	Foraminifera, Globothalamea
Elphidium Montfort, 1808	Foraminifera, Globothalamea
Globocassidulina crassa (d'Orbigny, 1839)	Foraminifera, Globothalamea
Hyalinea balthica (Schröter in Gmelin, 1791)	Foraminifera, Globothalamea

Melonis affinis (Reuss, 1851)	Foraminifera, Globothalamea
Nonionellina labradorica (Dawson, 1860)	Foraminifera, Globothalamea
Pullenia osloensis Feyling-Hanssen, 1954	Foraminifera, Globothalamea
Quinqueloculina stalkeri Loeblich & Tappan, 1953	Foraminifera, Tobothalamea
Stainforthia loeblichi (Feyling-Hanssen, 1954)	Foraminifera, Globothalamea
Stainforthia Hofker, 1956	Foraminifera, Globothalamea

Anomia ephippium Linnaeus, 1758	Molluca, Bivalva
Arctica islandica (Linnaeus, 1767)	Mollusca, Bivalva
Bathyarca glacialis (Gray, 1824)	Mollusca, Bivalva
Cerastoderma edule (Linnaeus, 1758)	Mollusca, Bivalva
Chlamys islandica (Müller, 1776)	Mollusca, Bivalva
Euspira montagui (Forbes, 1838)	Mollusca, Gastropoda
Glossus humanus (Linnaeus, 1758)	Mollusca, Bivalva
Hiatella arctica (Linnaeus, 1767)	Mollusca, Bivalva
Macoma calcarea (Gmelin, 1791)	Mollusca, Bivalva
Musculus discors (Linnaeus, 1767)	Mollusca, Bivalva
Mya truncata Linnaeus, 1758	Mollusca, Bivalva
Mytilus edulis Linnaeus, 1758	Mollusca, Bivalva
Mytilus trossulus Gould, 1850	Mollusca, Bivalva

Nuculana pernula (Müller, 1779)	Mollusca, Bivalva
Portlandia arctica (Gray, 1824)	Mollusca, Bivalva
Pseudamussium peslutrae (Linnaeus, 1771)	Mollusca, Bivalva
Ruditapes philippinarum (Adams & Reeve, 1850)	Mollusca, Bivalva
Roxania utriculus (Brocchi, 1814)	Mollusca, Gastropoda
Scrobicularia plana (da Costa, 1778)	Mollusca, Bivalva
Similipecten greenlandicus (Sowerby II, 1842)	Mollusca, Bivalva
Yoldiella lenticula (Møller, 1842)	Mollusca, Bivalva